

# OmniStream: Mastering Perception, Reconstruction and Action in Continuous Streams

Yibin Yan<sup>1,2,\*</sup>, Jilan Xu<sup>3,\*</sup>, Shangzhe Di<sup>1</sup>, Haoning Wu<sup>1</sup>, Weidi Xie<sup>1</sup>

<sup>1</sup>School of Artificial Intelligence, SJTU, <sup>2</sup>Shanghai Innovation Institute, <sup>3</sup>VGG, Oxford

\*Joint first author

Modern visual agents require representations that are general, causal, and physically structured to operate in real-time streaming environments. However, current vision foundation models remain fragmented, specializing narrowly in image semantic perception, offline temporal modeling, or spatial geometry. This paper introduces **OmniStream**, a unified streaming visual backbone that effectively perceives, reconstructs, and acts from diverse visual inputs. By incorporating causal spatiotemporal attention and 3D rotary positional embeddings (3D-RoPE), our model supports efficient, frame-by-frame online processing of video streams via a persistent KV-cache. We pre-train **OmniStream** using a synergistic multi-task framework coupling static and temporal representation learning, streaming geometric reconstruction, and vision-language alignment on 29 datasets. Extensive evaluations show that, even with a strictly frozen backbone, **OmniStream** achieves consistently competitive performance with specialized experts across image and video probing, streaming geometric reconstruction, complex video and spatial reasoning, as well as robotic manipulation (unseen at training). Rather than pursuing benchmark-specific dominance, our work demonstrates the viability of training a single, versatile vision backbone that generalizes across semantic, spatial, and temporal reasoning, *i.e.*, a more meaningful step toward general-purpose visual understanding for interactive and embodied agents.

Page: <https://go2heart.github.io/omnistream>

Code: <https://github.com/Go2Heart/OmniStream>



## 1 Introduction

Modern visual agents are increasingly deployed in *streaming* settings: a robot observes the world through a camera, an assistant watches a video, or an AR device processes an egocentric feed. In such cases, the agent must update its beliefs online from a continuous stream, under tight latency and memory budgets. A useful representation must therefore be (i) *general*, supporting recognition, reasoning, and interaction; (ii) *causal*, depending only on past and present frames; and (iii) *structured*, capturing not only appearance but also geometry and motion.

In the language community, models achieve generality with a single autoregressive backbone trained under next-token prediction [1, 16, 90]. This works not merely due to scale, but because the diverse tasks can share a common representation and training interface. Vision, however, remains far less unified. The tasks differ not only in supervision but also in the nature of their outputs: discrete labels [26], segmentation masks [43], dense depth [102], 3D geometry [84], and temporally evolving predictions. As a result, the field has converged on specialized foundation models: image encoders (*e.g.*, DINO [59, 74], SigLIP [82, 110]), video models (*e.g.*, V-JEPA [6, 10], VideoMAE [81, 85]), and geometric experts (*e.g.*, DepthAnything [49, 102, 103], VGGT [84]). While effective in-domain, these models typically learn representations tailored to a narrow objective (semantic invariances, temporal motion, or spatial geometry), and do not directly yield a single backbone that transfers across *static semantics*, *temporal dynamics*, and *3D structure*—especially in an online, causal regime.

A natural direction is to “unify” vision by converting everything into text-like token generation, as explored by Florence [95, 109], OFA [86], and Unified-IO [54, 55]. These models provide a convenient interface, but the unification still largely happens at the *output* level. In practice, accommodating new tasks often requires expensive re-training, re-tokenization of outputs, or architectural adjustments to the generative head. This leaves an open question that is more representation-centric than interface-centric: Can we learn a *single*

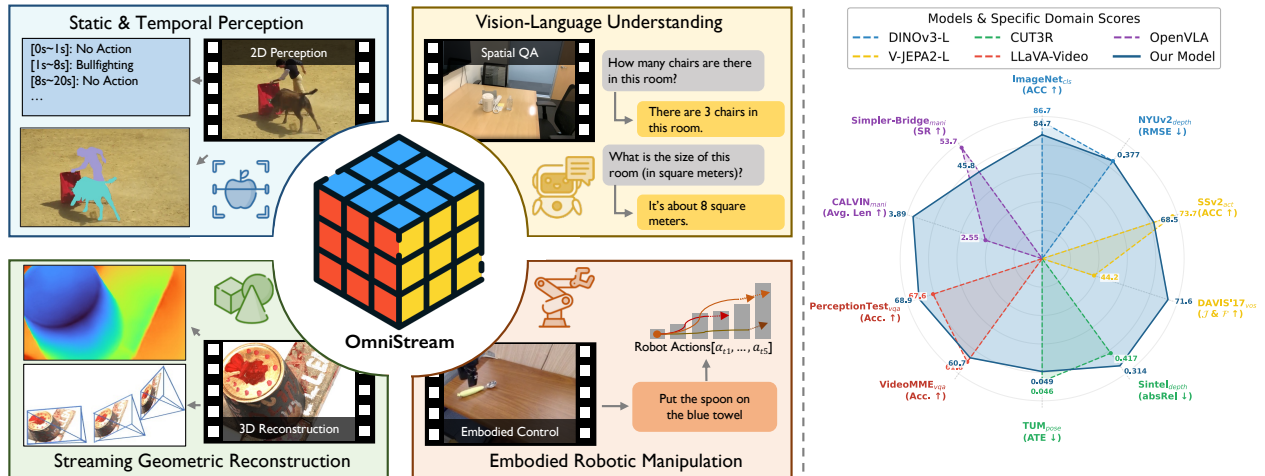


**Figure 1** Left: **OmniStream** supports a wide spectrum of tasks, including 2D/3D perception, vision-language understanding, and embodied robotic manipulation. Right: the frozen features of our single backbone achieve highly competitive or superior performance compared to leading domain-specific experts.

*streaming visual backbone* whose representations are sufficiently universal that many downstream tasks can be solved on top of it, without modifying or fine-tuning the backbone?

In this paper, we propose **OmniStream**, a unified streaming visual backbone that turns a strong pre-trained image model into an online, temporally causal model while preserving its spatial priors. OmniStream is built around two design choices. First, we introduce **causal spatiotemporal attention**, which enforces strict temporal causality and enables efficient frame-by-frame inference via a persistent KV-cache, avoiding re-computation over past frames. Second, we propose **3D rotary positional embeddings (3D-RoPE)**, which extends the 2D RoPE to a *spatiotemporal* relative encoding, allowing the model to reason about where-and-when across long streams.

Architecture alone, however, does not guarantee universality: the representation needs to be *trained* to encode what downstream tasks need. To this end, we adopt a unified pre-training recipe that couples three complementary signals, each targeting a different axis of *understanding*: **i) static and temporal representation learning**: a self-supervised student-teacher distillation objective that unifies image representation learning with causal video modeling. By distilling both global (image/video-level) and local (patch-level) features, the backbone learns semantic invariances and motion-sensitive dynamics while respecting causality; **ii) streaming geometric reconstruction**: lightweight feedforward dual DPT and camera heads predict depth maps, ray maps, and camera poses from the stream, injecting explicit 3D constraints so that the representation reflects physical scene structure rather than appearance alone; **iii) vision-language alignment**: a lightweight auto-regressive language decoder trained on captioning, OCR, and visual grounding connects visual tokens with linguistic concepts, encouraging fine-grained details and semantic grounding that are useful for reasoning-heavy tasks. Together, these objectives encourage OmniStream to learn representations that are simultaneously temporally coherent, geometrically grounded, and language-aligned.

In summary, we propose **OmniStream**, a unified *streaming* visual backbone that extends a pre-trained image encoder with causal spatiotemporal attention and 3D-RoPE, enabling strictly causal, efficient online inference. Our extensive multi-task pre-training across 29 diverse datasets demonstrate that scaling diverse objectives is highly synergistic rather than merely additive: (i) causal video modeling is essential for capturing dynamic motions; (ii) explicit geometric pre-training is prerequisite for downstream spatial intelligence and embodied control; and (iii) early vision-language alignment within the backbone is critical to prevent catastrophic failures during VLM integration. Lastly, we demonstrate that OmniStream serves as a strong **vision backbone**: its features perform well on standard image/video probing, it natively supports competitive streaming geometric reconstruction, and it enables downstream language models and policy heads to solve general and complex spatial video question answering, and robotic manipulation without backbone fine-tuning, matching or surpassing task-specific baselines. We will release the **model and training code** to the community.

## 2 Related Work

**Vision foundation models.** The pursuit of a unified vision foundation model capable of generalizing across diverse perceptual dimensions remains a central objective in computer vision. For static images, vision-language contrastive learning frameworks such as CLIP [67] and SigLIP [82, 110] have demonstrated impressive semantic generalization, while self-supervised paradigms like DINO [20, 59, 74], MAE [33], and I-JEPA [5] excel in extracting low-level visual features. In the video domain, research has pivoted toward capturing complex spatiotemporal dependencies. Supervised models [3, 12, 98] leverage large-scale video-text corpora, whereas self-supervised approaches focus on reconstructing masked spatiotemporal patches at the pixel level [81, 85] or feature level [6, 10]. Despite these advancements, the landscape remains fragmented: most models are either restricted to static perception or rely on non-causal, offline temporal processing. Our OmniStream bridges this gap by unifying image and video representation learning within a strictly causal, streaming framework.

**Feed-forward 3D reconstruction models.** DUST3R [88] has led a paradigm shift in multi-view geometry, moving from traditional optimization-based methods like Structure-from-Motion (SfM) to learning-based feed-forward neural networks. Building upon this, subsequent works have extended this paradigm to support multi-view and video inputs beyond simple image pairs [49, 84, 91, 100, 111]. Parallel to these developments, the research focus has transitioned from offline sequence reconstruction to the more challenging *online* setting [44, 83, 87, 93, 120], which requires real-time geometric reasoning. Although these specialized 3D experts demonstrate remarkable precision in geometric tasks, they often lack high-level semantic reasoning capabilities. Our method not only achieves competitive performance in streaming geometric estimation but also exhibits superior generalization across vision tasks that require deep semantic understanding, effectively bridging the gap between spatial structure and semantic abstraction.

**Visual representation for VLMs and VLAs.** Advanced Vision-Language Models (VLMs) [7, 9, 45, 51, 52, 114] rely on robust visual encoders to ground textual reasoning. While contrastive models like CLIP [67] and SigLIP [110] serve as the *de facto* standard for global semantics, they typically fall short in fine-grained visual perceptions [80]. Recent studies have sought to enhance visual representations by adopting more powerful backbones [2, 8, 82], leveraging ensembles of multiple specialized encoders [38, 53, 72, 79], or incorporating specialized geometric experts to bolster spatial understanding [27, 115]. Building on general VLMs, Vision-Language-Action (VLA) models [14, 41, 121] demand both high-level semantics and low-level geometric precision. However, a significant gap exists between current VLMs and the demands of VLA embodied tasks [47], especially in visual representation [112]. In contrast, our OmniStream bridges this gap by unifying semantic, dynamic and geometric representations into a single, efficient streaming backbone.

## 3 Method

This section presents **OmniStream**, a unified *streaming* visual backbone. We formalize causal streaming perception in Sec. 3.1, describe the backbone that turns a pre-trained image ViT into an efficient online encoder in Sec. 3.2, introduce our multi-task training framework in Sec. 3.3, and detail how the learned representation supports unified perception, reasoning, and action in Sec. 3.4.

### 3.1 Problem Formulation

We aim to train a **unified streaming visual backbone** that produces a general-purpose representation at each time step of a video stream and can be reused by diverse downstream tasks with minimal task-specific modeling.

Formally, let a continuous video stream be  $\mathcal{V}^T = \{\mathcal{I}_1, \mathcal{I}_2, \dots, \mathcal{I}_T\}$ , where  $\mathcal{I}_t \in \mathbb{R}^{H \times W \times 3}$ . At time step  $t$ , the backbone processes the current frame and historical context to produce a composite output state  $\mathbf{O}_t$ :

$$\mathbf{O}_t = f_\theta(\mathcal{I}_t \mid \mathcal{I}_1, \dots, \mathcal{I}_{t-1}), \quad t \in \{1, \dots, T\}. \quad (1)$$

To support real-time deployment, we enforce a **strict causality constraint**:  $\mathbf{O}_t$  must not depend on future frames  $\{\mathcal{I}_{t+1}, \dots, \mathcal{I}_T\}$ . The same backbone is expected to support multiple regimes:

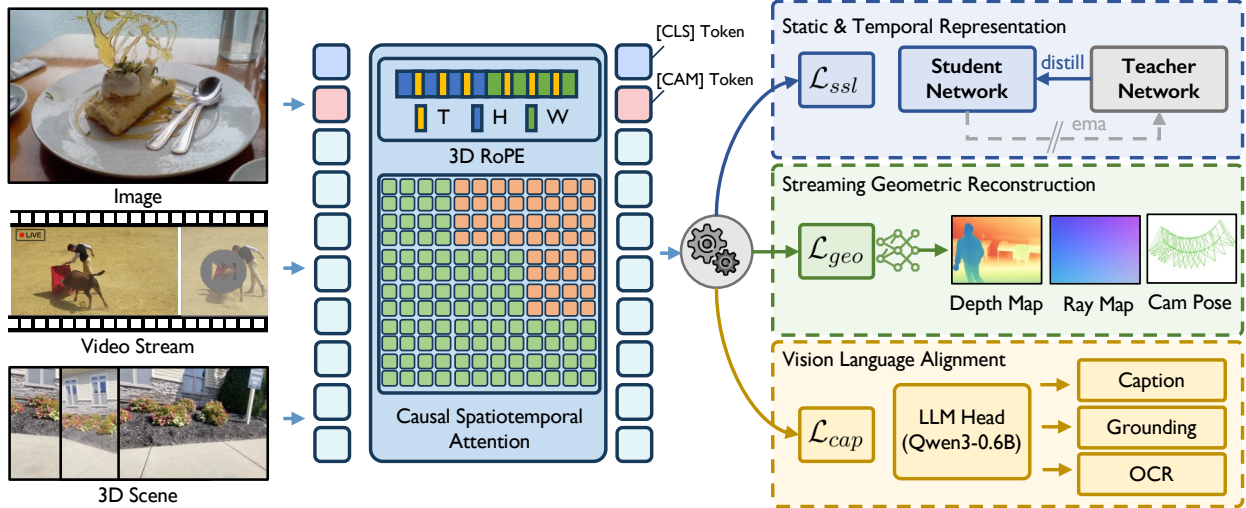


**Figure 2 Overall framework of OmniStream.** Equipped with 3D-RoPE and causal spatiotemporal attention, our unified backbone is trained via a multi-task framework that couples static and temporal representation learning, streaming geometric reconstruction, and vision-language alignment.

- i) **Static perception** ( $T = 1$ ): the stream degenerates to a single image; the model acts as an image encoder capturing semantics and layout;
- ii) **Dynamic understanding** ( $T > 1$ ): the backbone captures temporal evolution and motion cues from a continuous stream;
- iii) **Geometric reasoning** ( $T > 1$ ): by aggregating multi-frame evidence causally, the backbone supports online reconstruction of 3D/4D scene structure;
- iv) **Embodied control** ( $T \geq 1$ ): the backbone supplies real-time, action-oriented representation to drive closed-loop policies for robotic manipulation.

### 3.2 Streaming Visual Backbone

**Overview.** We instantiate **OmniStream** as a vision transformer from DINOv3 [74], leveraging its strong spatial representation as a starting point. As depicted in Fig. 2, to evolve an image encoder into a **unified streaming** backbone, we introduce two modifications: (i) **causal spatiotemporal attention** to enable online inference with temporal causality and a persistent KV-cache; (ii) **3D rotary positional embeddings (3D-RoPE)**, extending the 2D positional priors to the spatiotemporal domain. These changes allow efficient processing of long streams while preserving the pre-trained spatial inductive bias.

**Tokenization and outputs.** For a video stream  $\mathcal{V}^T \in \mathbb{R}^{T \times H \times W \times 3}$ , we split each frame into non-overlapping  $p \times p$  patches, producing  $h \times w$  patches per frame with  $h = H/p$  and  $w = W/p$ . After linear projection, we prepend per-frame special tokens: one global [CLS] token, four register tokens [25], and an optional [CAM] token. Let  $N_s$  be the number of special tokens per frame; the input sequence is  $\mathbf{z}^0 \in \mathbb{R}^{T \times (N_s + hw) \times d}$ .

After multiple Transformer blocks, we extract (i) dense spatiotemporal feature maps from selected intermediate layers  $\mathbf{L}$ , and (ii) final-layer special tokens for global semantics and camera prediction:

$$\mathbf{O} = \{\mathcal{Z}, \mathbf{z}_{cls}, \mathbf{z}_{cam}\} = f_{\theta}(\mathbf{z}^0), \quad (2)$$

where  $\mathcal{Z}$  denotes selected layers' dense patch feature  $\{\mathbf{z}^{(\ell)} \in \mathbb{R}^{T \times h \times w \times d}\}_{\ell \in \mathbf{L}}$ , the last-layer [CLS] token  $\mathbf{z}_{cls} \in \mathbb{R}^{T \times d}$  provides an image/video-level summary, and the [CAM] token  $\mathbf{z}_{cam} \in \mathbb{R}^{T \times d}$  is routed to the camera head for pose estimation.

**Causal spatiotemporal attention.** A naive Transformer that attends over all frames violates causality and is inefficient for streaming. We therefore apply spatiotemporal self-attention with a **causal temporal mask**, so tokens at time  $t$  may only attend to tokens from times  $\leq t$ .

Let the total number of tokens be  $N_{\text{total}} = T \cdot (N_s + hw)$ , the attention mask as  $\mathbf{M} \in \{0, -\infty\}^{N_{\text{total}} \times N_{\text{total}}}$ . The masked attention is formalized as:

$$\text{Attn}(\mathbf{Q}, \mathbf{K}, \mathbf{V}) = \text{Softmax}\left(\frac{\mathbf{Q}\mathbf{K}^\top}{\sqrt{d_{\text{head}}}} + \mathbf{M}\right) \mathbf{V}, \quad (3)$$

For a query token with global index  $u$  and a key token with global index  $v$ , the mask is defined via a frame-index mapping  $\tau(\cdot)$ :

$$M_{u,v} = \begin{cases} 0, & \text{if } \tau(u) \geq \tau(v) \\ -\infty, & \text{if } \tau(u) < \tau(v) \end{cases}, \quad (4)$$

where  $\tau(u)$  returns the time step of token  $u$ . This ensures every patch in frame  $t$  can attend to all patches in frames  $\leq t$ , but never to future frames.

**Streaming inference with KV-cache.** Under the above causality, inference can be performed incrementally: when frame  $t$  arrives, we compute its queries and reuse cached keys/values from frames  $\leq t - 1$ . This yields online processing without recomputing attention over the full past stream, while producing the same output as full causal attention.

**3D rotary positional embeddings (3D-RoPE).** The original DINOv3 [74] uses 2D RoPE to encode relative spatial offsets. We extend RoPE to the spatiotemporal domain by re-purposing the per-head feature dimension  $d_{\text{head}}$  while preserving as much pre-trained spatial structure as possible. Concretely, we adopt an allocation strategy with a **2:3:3** split across  $(t, y, x)$ , namely, time, height, and width. We interleave temporal components into the original 2D RoPE such that indices  $i \equiv 3 \pmod{4}$  encode time  $t$  [8], while the remaining indices follow the original DINOv3 pattern for  $y$  and  $x$ . We further apply RoPE-box jittering [74] to improve robustness of the positional embeddings.

### 3.3 Unified Multi-task Learning Objectives

A unified streaming backbone should ideally produce representations that transfer seamlessly across semantics, dynamics, geometry, and language. We therefore train OmniStream with a unified multi-task framework that combines three complementary objectives: **static & temporal representation learning**, **streaming geometric reconstruction**, and **vision-language alignment**. These signals are designed to be compatible with causal streaming environments and to encourage representations that are simultaneously discriminative, temporally coherent, and physically grounded.

**Static & temporal representation learning.** We treat an image as a degenerate stream with  $T = 1$ , enabling a single objective to cover both images and videos. We employ a DINOv3-style student-teacher distillation objective [74]:

$$\mathcal{L}_{\text{ssl}} = \mathcal{L}_{\text{DINO}} + \mathcal{L}_{\text{iBOT}} + 0.1 \times \mathcal{L}_{\text{KoLeo}} + \mathcal{L}_{\text{gram}}, \quad (5)$$

Given a set of views (global/local crops from an image or a video clip), the four terms encourage (i) global semantic consistency ( $\mathcal{L}_{\text{DINO}}$ ) [20], (ii) patch-level discriminative features ( $\mathcal{L}_{\text{iBOT}}$ ) [118], (iii) a well-spread feature space ( $\mathcal{L}_{\text{KoLeo}}$ ) [71], and (iv) a consistent patch-level feature during training ( $\mathcal{L}_{\text{gram}}$ ) [74]. We provide full formulations in the appendix.

**Streaming geometric reconstruction.** To inject explicit 3D constraints, we attach feed-forward geometric heads that reconstruct monocular streams into a coherent dynamic representation. We use: (i) a depth head implemented as a dual-DPT module [49] to predict dense depth maps and ray maps; and (ii) a lightweight MLP camera head to predict camera poses.

Using the selected backbone features  $\{\mathbf{z}^{(\ell)} \in \mathbb{R}^{T \times h \times w \times d}\}_{\ell \in \mathbf{L}}$ , the depth head predicts depth maps  $\hat{D} \in \mathbb{R}^{T \times H \times W \times 1}$  and ray maps  $\hat{R} \in \mathbb{R}^{T \times H \times W \times 6}$ . The camera head consumes camera tokens  $\mathbf{z}_{\text{cam}}$  and predicts per-frame pose parameters  $\hat{g} \in \mathbb{R}^{T \times 9}$ , which is the concatenation of the rotation quaternion  $\mathbf{q} \in \mathbb{R}^{T \times 4}$ , the translation vector  $\mathbf{t} \in \mathbb{R}^{T \times 3}$ , and the field of view  $\mathbf{f} \in \mathbb{R}^{T \times 2}$ , with the camera’s principal point assumed to be at the image center. Following [84], we supervise these outputs against normalized ground-truth depth maps  $D$ , ray maps  $R$ , point maps  $P$ , and camera poses  $g$  and perform a multi-task geometric loss:

$$\mathcal{L}_{\text{geo}} = \mathcal{L}_{\text{depth}} + \mathcal{L}_{\text{ray}} + \mathcal{L}_{\text{points}} + \mathcal{L}_{\text{camera}}, \quad (6)$$

**Depth with confidence.** We use an L1 regression loss with an additional gradient term and a learned confidence  $c_t$ :

$$\mathcal{L}_{\text{depth}} = \sum_{t=1}^T \left( \|c_t(\hat{D}_t - D_t)\|_1 + \|c_t(\nabla\hat{D}_t - \nabla D_t)\|_1 - \alpha \log c_t \right), \quad (7)$$

where  $\nabla$  is the spatial gradient operator and  $\alpha$  is a hyper-parameter.

**Rays, points, and camera.** Similarly, we apply standard L1 regression to ray maps, point maps, and camera poses:

$$\mathcal{L}_{\text{ray}} = \sum_{t=1}^T \|\hat{R}_t - R_t\|_1, \quad \mathcal{L}_{\text{points}} = \sum_{t=1}^T \|\hat{P}_t - P_t\|_1, \quad \mathcal{L}_{\text{camera}} = \sum_{t=1}^T \|\hat{g}_t - g_t\|_1 \quad (8)$$

where the camera ray is defined by concatenating the ray origin  $\mathbf{o} \in \mathbb{R}^3$  and direction  $\mathbf{d} \in \mathbb{R}^3$ . And point maps can thus be derived as  $\hat{P}_t = \hat{\mathbf{o}}_t + \hat{D}_t \odot \hat{\mathbf{d}}_t$ .

**Vision-language alignment.** To align visual tokens with linguistic concepts and enable reasoning-oriented downstream tasks, we attach an MLP projector and lightweight autoregressive language decoder (Qwen3-0.6B [99]) to the vision backbone. This branch is trained on a mixture of vision-language tasks including dense captioning, OCR, and object grounding.

Given the visual tokens from the last layer  $\mathbf{z}^L$  and an instruction prompt  $\mathbf{x}_{\text{inst}}$ , we train with the standard language modeling objective:

$$\mathcal{L}_{\text{cap}} = - \sum_{n=1}^{L_{\text{text}}} \log P_{\text{text}}(y_n | \mathbf{z}^L, \mathbf{x}_{\text{inst}}, \mathbf{y}_{<n}), \quad (9)$$

where  $P_{\text{text}}$  is the token distribution predicted by the decoder and  $\mathbf{y}_{<n}$  denotes previously generated tokens. During training, gradients are back-propagated through the language decoder into the vision backbone, injecting fine-grained semantic and spatial supervision, which proves to be essential capabilities for VLM and VLA integration in our experiments.

**Total objective.** The overall training loss is a weighted combination:

$$\mathcal{L}_{\text{total}} = \lambda_{\text{ssl}} \cdot \mathcal{L}_{\text{ssl}} + \lambda_{\text{geo}} \cdot \mathcal{L}_{\text{geo}} + \lambda_{\text{cap}} \cdot \mathcal{L}_{\text{cap}}, \quad (10)$$

where we set  $\lambda_{\text{ssl}} = 0.1$  and  $\lambda_{\text{geo}} = \lambda_{\text{cap}} = 1$  to balance the loss magnitudes.

### 3.4 Universal Representation for Downstream Applications

A foundation vision backbone should be reusable without expensive full-model adaptation. Accordingly, we evaluate OmniStream in a **strictly frozen** setting, where the backbone parameters are kept fixed and only specific task modules are trained. We organize downstream tasks into three increasing levels of complexity:

**Perception: image & video.** For discriminative perception tasks, we attach lightweight heads on top of frozen vision features. For static image tasks (*e.g.*, segmentation), we apply linear decoders on spatial tokens; for video tasks, we use attentive pooling modules on the frozen spatiotemporal features.

**Reasoning: vision-language models (VLM).** To enable spatial and temporal reasoning, we integrate OmniStream with an LLM by using an MLP projector that maps frozen visual tokens into the language embedding space. The LLM then generates text conditioned on the projected visual context and textual instructions. Throughout, the vision backbone remains frozen, forcing the LLM to interpret the intrinsic visual representation.

**Action: vision-language-action (VLA).** For embodied control, we extend the VLM setup by attaching an MLP-based action expert to the LLM outputs to predict robot actions  $a_t$  from the frozen visual observations and language instructions. Crucially, because our pre-training objectives ( $\mathcal{L}_{\text{ssl}}, \mathcal{L}_{\text{geo}}$ ) explicitly encode dynamics and geometry, the frozen features provide a strong bridge from perception to action without domain-specific visual fine-tuning.

Task	Pre-training Dataset	Frames
<b>Image SSL</b>	DataComp-100M [30], ImageNet-21K [69]	~113M
<b>Video SSL</b>	Kinetics [21], SSv2 [32], PE-Videos [15]	~20M
<b>3D/4D Scenes</b>	Co3Dv2 [68], WildRGBD [94], BlendedMVS [106], MegaDepth [48], MVS-Synth [36], PointOdyssey [116], HyperSim [70], TartanAir [89], DL3DV [50], ScanNet [23], ScanNet++ [107], ArkitScenes [11], Virtual Kitti 2 [19], MapFree [4], Dynamic Replica [39], Spring [58], OmniWorld-Games [119], Aria Synthetic Environments [62], Waymo-Open [77]	~18M
<b>Captioning</b>	GRIT [18, 64], RefCOCO Series [40], Blip3-OCR [97], SA1B-Caption [22]	~50M
<b>Total</b>	-	~200M

**Table 1 Overview of pre-training datasets.** We leverage a diverse collection of images, videos, and 3D/4D data.

## 4 Experiments

### 4.1 Pre-training Data

We train our model on a wide range of datasets featuring static images, dynamic videos, and geometric 3D/4D Scenes. Totally, our training pipeline consumes approximately 200M frames from 29 datasets, providing a dense and diverse supervisory signal that ensures the model’s robustness across various streaming scenarios. A detailed breakdown of the pre-training data is provided in Tab. 1.

### 4.2 Implementation Details

We initialize our model using the pre-trained weights of DINOv3 [74] ViT-L. We employ a multi-task learning strategy combined with gradient accumulation, where we sequentially interleave all tasks within each training step and perform a single model parameter update after traversing the batches from all tasks. The training is conducted on  $64 \times$  NVIDIA H200 GPUs and is divided into two stages: the first trained for 60K steps at a resolution of  $224 \times 224$ , followed by a second stage trained for 120K steps at a resolution of  $512 \times 512$ . For optimization, we use Adam optimizer [42] with a peak learning rate of  $1 \times 10^{-4}$ , employing a 4K-step warmup followed by a cosine annealing schedule. Weight decay is disabled in both stages. All multi-frame sequences, including video and geometric scenes, are sampled with a sequence length of  $T = 16$  frames per sample. Benefiting from our causal mask design, each training sample effectively provides distinct supervision signals for varying temporal contexts ranging from 1 to  $T$  frames.

### 4.3 Downstream Evaluations

To validate the universality and robustness of our learned representations, we structure our downstream experiments into four phases, as illustrated in Tab. 2: (i) **image & video probing**, which assesses the quality of global and dense features on standard image and video benchmarks; (ii) **streaming geometric reconstruction**, which evaluates the model’s capability to estimate continuous camera poses and depth maps in an online fashion; (iii) **visual backbone for VLMs**, which incorporates the representation into Vision-Language Models (VLMs) for complex video and spatial reasoning; and (iv) **visual backbone for VLA policies**, where the model serves as the visual engine for Vision-Language-Action (VLA) policies in robotic manipulation. Crucially, to demonstrate its capacity as a truly universal foundational vision model, **we keep the backbone strictly frozen** across all downstream tasks.

**Image & video probing.** We first evaluate the versatility of the frozen features extracted by OmniStream across both static and dynamic domains. Following the DINOv3 [74] protocol for image tasks, we train task-specific linear heads on top of the frozen backbone to evaluate ImageNet-1K [26] classification, ADE20K [117] semantic segmentation, and NYUv2 [73] monocular depth estimation. For video understanding, we probe action recognition on Kinetics-400 (K400) [21] and Something-Something V2 (SSv2) [32] using attentive pooling from the V-JEPA 2 [6] setup. Furthermore, we evaluate dense spatiotemporal tracking on the DAVIS’17 [65] Video Object Segmentation (VOS) benchmark.

	Benchmark	Ours	DINOv3-L	V-JEPA2-L	CUT3R	LLaVA-Video	OpenVLA
<i>Image</i>	<b>ImageNet</b> <sub>cls</sub> ↑	84.7	86.7	-	-	-	-
	<b>NYUv2</b> <sub>monodepth</sub> ↓	0.377	0.377	-	-	-	-
	<b>ADE20K</b> <sub>seg</sub> ↑	49.1	51.5	-	-	-	-
<i>Video</i>	<b>SSv2</b> <sub>act</sub> ↑	68.5	54.0	73.7	-	-	-
	<b>K400</b> <sub>act</sub> ↑	85.7	83.6	85.1	-	-	-
	<b>DAVIS'17</b> <sub>vos</sub> ↑	71.6	73.2	44.2	-	-	-
<i>3D Geom.</i>	<b>Sintel</b> <sub>videodepth</sub> ↓	0.314	-	-	0.421	-	-
	<b>BONN</b> <sub>videodepth</sub> ↓	0.072	-	-	0.078	-	-
	<b>KITTI</b> <sub>videodepth</sub> ↓	0.136	-	-	0.118	-	-
	<b>Sintel</b> <sub>pose</sub> ↓	0.227	-	-	0.213	-	-
	<b>TUM</b> <sub>pose</sub> ↓	0.049	-	-	0.046	-	-
	<b>ScanNet</b> <sub>pose</sub> ↓	0.076	-	-	0.099	-	-
<i>VLM</i>	<b>VideoMME</b> <sub>vqa</sub> ↑	60.7	-	-	-	61.8	-
	<b>VideoMMU</b> <sub>vqa</sub> ↑	40.0	-	-	-	38.7	-
	<b>PerceptionTest</b> <sub>vqa</sub> ↑	68.9	-	-	-	67.6	-
	<b>EgoSchema</b> <sub>vqa</sub> ↑	60.9	-	-	-	57.3	-
	<b>VSI-Bench</b> <sub>vqa</sub> ↑	70.6	-	-	-	35.6	-
<i>VLA</i>	<b>CALVIN</b> <sub>mani</sub> ↑	3.89	-	-	-	-	2.55
	<b>Simpler-Bridge</b> <sub>mani</sub> ↑	45.8	-	-	-	-	53.7

**Table 2 Holistic evaluation.** We compare OmniStream across 5 domains. Subscripts denote the specific task (*i.e.*, cls: classification, monodepth: monocular depth estimation, seg: semantic segmentation, act: video action recognition, vos: video object segmentation, videodepth: video depth estimation, pose: camera pose estimation, vqa: visual question answering, mani: robotic manipulation). The evaluated metrics are ACC@1 for cls and act, RMSE for monodepth, mIOU for seg,  $\mathcal{J}\&\mathcal{F}$  for vos, absRel for videodepth, ATE for pose, Accuracy (Acc.) for vqa, Average Length (Avg. Len) for CALVIN, and Success Rate (SR %) for Simpler-Bridge. Here, “-” indicates that a specialized baseline is not natively applicable to or lacks the capability for the given task.

As presented in Tab. 2, OmniStream successfully bridges the gap between static and dynamic perception. On image benchmarks, it preserves robust spatial discrimination, achieving competitive results on dense prediction tasks (NYUv2 and ADE20K) comparable to the image specialist DINOv3. In contrast, OmniStream demonstrates superior temporal understanding ability, significantly outperforming DINOv3 on the motion-intensive SSv2 dataset (68.5% vs. 54.0%). Unlike typical video backbones that exhibit poor spatial alignment (*e.g.*, V-JEPA 2 at 44.2  $\mathcal{J}\&\mathcal{F}$ ), OmniStream leverages the KV-cache to enable a long-range extraction of the entire video. Our approach yields a  $\mathcal{J}\&\mathcal{F}$  mean of 71.6, performing on par with leading image-based per-frame extractors (DINOv3 at 73.2). This confirms that our unified multi-task training effectively injects temporal motion dynamics into the representations, without compromising the fine-grained spatial priors required for dense image tasks.

**Streaming geometric reconstruction.** To evaluate the geometric ability of our streaming representations, we benchmark OmniStream on online 3D reconstruction tasks following CUT3R [87]. We assess online video depth estimation across Sintel [17], BONN [61], and KITTI [31] (Tab. 3), and online camera pose estimation on Sintel, TUM Dynamics [76], and ScanNet [23] (Tab. 4).

Across both tasks, our unified encoder consistently establishes highly competitive or superior results against specialized online 3D models, validating its robustness in real-time spatial perception. Notably, benefiting from our causal temporal attention mechanism, the architecture natively supports KV-caching during inference. This allows the model to process incoming video streams frame-by-frame with  $O(T)$  temporal complexity per step, avoiding the redundant re-computation typical of bidirectional global attention. Furthermore, by leveraging the geometric extrapolation properties inherent to our 3D-RoPE, OmniStream can seamlessly generalize to much longer, unseen sequences that significantly exceed the training horizon. For instance, although OmniStream is pre-trained with a fixed temporal window of only  $T = 16$  frames, it demonstrates impressive zero-shot length extrapolation capabilities, effortlessly processing continuous streams of up to 110

Method	Param.	Sintel		BONN		KITTI	
		Abs Rel↓	$\delta < 1.25\uparrow$	Abs Rel↓	$\delta < 1.25\uparrow$	Abs Rel↓	$\delta < 1.25\uparrow$
Span3R [83]	600M	0.622	42.6	0.144	81.3	0.198	73.7
Cut3R [87]	600M	<u>0.421</u>	<u>47.9</u>	0.078	93.7	<u>0.118</u>	<u>88.1</u>
Point3R [93]	600M	0.481	44.8	<b>0.066</b>	<u>95.8</u>	<b>0.093</b>	<b>93.5</b>
<b>Ours</b>	400M	<b>0.314</b>	<b>58.3</b>	<u>0.072</u>	<b>96.7</b>	0.136	81.8

Table 3 Comparison on online video depth estimation.

Method	Param.	Sintel			TUM-dynamics			ScanNet		
		ATE↓	RPE <sub>T</sub> ↓	RPE <sub>R</sub> ↓	ATE↓	RPE <sub>T</sub> ↓	RPE <sub>R</sub> ↓	ATE↓	RPE <sub>T</sub> ↓	RPE <sub>R</sub> ↓
Span3R [83]	600M	0.329	0.110	4.471	0.056	0.021	<u>0.591</u>	<u>0.096</u>	0.023	0.661
Cut3R [87]	600M	<b>0.213</b>	<u>0.066</u>	<b>0.621</b>	<b>0.046</b>	<u>0.015</u>	<b>0.473</b>	<u>0.099</u>	<u>0.022</u>	<b>0.600</b>
Point3R [93]	600M	0.442	0.154	1.897	0.058	0.031	0.758	0.097	0.035	2.791
<b>Ours</b>	400M	<u>0.227</u>	<b>0.051</b>	<u>0.695</u>	<u>0.049</u>	<b>0.012</b>	0.601	<b>0.076</b>	<b>0.017</b>	<u>0.659</u>

Table 4 Comparison on online video camera pose estimation.

frames during evaluation.

**Visual backbone for VLMs.** Adhering to the framework of LLaVA-Video [114], we evaluate the efficacy of OmniStream as a general-purpose visual encoder for Video LLMs. We integrate our backbone with Qwen2.5-7B-Instruct [66] to perform general and spatial video question answering. Further training details are provided in the appendix.

As shown in the *VLM* section of Tab. 2, despite a frozen visual encoder and an identical general video data recipe, OmniStream achieves better performance than LLaVA-Video on general Video QA benchmarks. Although marginally behind on VideoMME [29], it consistently achieves superior results across other major benchmarks like VideoMMU [34], PerceptionTest [63], and EgoSchema [56], highlighting its effectiveness. Our model further demonstrates exceptional spatial reasoning capabilities. As shown in Tab. 5, on the **VSI-Bench** [101], a challenging benchmark for spatial intelligence, our model achieves state-of-the-art performance. Remarkably, it surpasses specialized geometry-aware baselines equipping extra geometry encoders, such as VLM-3R [27] and SpaceMind [115]. This result strongly validates that our unified streaming pre-training naturally engenders rich, actionable spatial understanding within the visual features themselves, eliminating the need for auxiliary geometric modules.

**Visual backbone for VLA policies.** Finally, we extend our evaluation to Embodied AI, assessing OmniStream as the “perception brain” for VLA policies. Following VLM4VLA [112], we adapt OmniStream-7B into a Vision-Language-Action model by attaching a lightweight MLP action head, trained on two simulated robotic manipulation benchmarks: **CALVIN** (ABC-D split)[57] for long-horizon instruction following, and **SIMPLER-ENV** (Bridge V2 dataset)[46] for real-to-sim generalization.

Crucially, the visual encoder remains **fully frozen** during adaptation. As shown in Tab. 6 and Tab. 7, strong general-purpose VLMs like Qwen2.5-VL struggle significantly in this setting, failing to translate high-level semantic knowledge into precise low-level control signals, highlighting a critical *misalignment* between general visual features and the requirements of embodied interaction, such as depth perception and dynamics prediction. In contrast, OmniStream achieves strong performance even with a frozen backbone, reaching success rates of 3.885 on CALVIN and 45.8% on SIMPLER-ENV. This underscores the universality of our representation: by explicitly encoding 3D geometry and temporal dynamics during pre-training, OmniStream bridges the gap between perception and action. To the best of our knowledge, this is the **first visual encoder** to demonstrate such effective zero-shot transferability to VLA benchmarks without domain-specific visual fine-tuning, paving the way for more efficient and generalizable embodied agents.

Methods	Avg.	Obj. Count	Abs. Dist.	Obj. Size	Room Size	Rel. Dist	Rel. Dir.	Route Plan	Appr. Order
GPT-4o [37]	34.0	46.2	5.3	43.8	38.2	37.0	41.3	31.5	28.5
Gemini-1.5-Pro [78]	45.4	56.2	30.9	64.1	43.6	51.3	46.3	36.0	34.6
LLaVA-OneVision-7B [45]	32.4	47.7	20.2	47.4	12.3	42.5	35.2	29.4	24.4
LLaVA-Video-7B [114]	35.6	48.5	14.0	47.8	24.2	43.5	42.4	34.0	30.6
Qwen2.5-VL-7B [9]	32.7	34.5	19.4	47.6	40.8	32.8	24.5	32.5	29.4
SpaceR-7B [60]	43.5	61.9	28.6	60.9	35.2	38.2	46.0	31.4	45.6
VILASR-7B [92]	45.4	63.5	34.4	60.6	30.9	48.9	45.2	30.4	49.2
VLM-3R-7B [27]	60.9	70.2	49.4	69.2	67.1	65.4	80.5	<b>45.4</b>	40.1
VST-7B [104]	60.6	72.0	44.4	74.3	68.3	59.7	55.8	<u>44.9</u>	65.2
SpaceMind [115]	<u>69.6</u>	<b>73.3</b>	<b>61.4</b>	<b>77.3</b>	<u>74.2</u>	<u>67.2</u>	<b>88.4</b>	44.3	<u>70.5</u>
OmniStream-7B	<b>70.6</b>	<u>73.2</u>	<u>55.7</u>	<u>76.9</u>	<b>74.8</b>	<b>72.3</b>	<u>82.1</u>	<b>45.4</b>	<b>84.6</b>

Table 5 Comparison on VSI-Bench.

Model (VLM Backbone)	Task-1	Task-2	Task-3	Task-4	Task-5	Calvin $\uparrow$
Expert Vision-Language-Action Models						
OpenVLA* (Llama-2) [41]	0.792	0.644	0.499	0.368	0.245	2.548
pi0* (Paligemma-1) [14]	0.896	0.785	0.786	0.610	0.532	3.509
VLM with VLM4VLA Models (Full Fine-tuning)						
Qwen2.5VL-7B [9]	0.935	0.864	0.807	0.758	0.693	4.057
Qwen3VL-8B [8]	0.940	0.868	0.797	0.746	0.684	4.035
Paligemma-1-3B [13]	0.914	0.813	0.692	0.599	0.488	3.506
Paligemma-2-3B [75]	0.901	0.775	0.669	0.575	0.486	3.406
KosMos-2-1.7B [64]	0.878	0.721	0.591	0.498	0.408	3.096
VLM with VLM4VLA Models (Frozen Vision)						
Qwen2.5VL-7B	0.901	0.700	0.536	0.433	0.334	2.905
LLaVA-Video-7B	0.876	0.701	0.542	0.438	0.340	2.898
<b>OmniStream-7B</b>	<b>0.931</b>	<b>0.848</b>	<b>0.768</b>	<b>0.703</b>	<b>0.634</b>	<b>3.885</b>

Table 6 Comparison on CALVIN ABC-D. Entries marked with \* are expert VLAs modified in VLM4VLA settings.

#### 4.4 Ablation Study

To investigate the effects of multitask learning, we conduct experiments with different task configurations. For computational efficiency, all models in this study are evaluated using the checkpoints of Stage-1 pre-training at  $224 \times 224$  resolution. Tab. 8 demonstrates the indispensable role of each pre-training objective: **(i) video modeling (w/o VideoSSL)**: Omitting video data from  $\mathcal{L}_{ssl}$  severely degrades dynamic perception (SSv2 drops from 69.3% to 63.0%; DAVIS declines from 71.6 to 67.7) and embodied control (CALVIN drops from 3.80 to 3.42), confirming its necessity for capturing dynamic motions. **(ii) geometric reconstruction (w/o 3D Geometry)**: Disabling the streaming geometric reconstruction objective collapses spatial perception (NYUv2 RMSE worsens to 0.471; ADE20K drops 7.3 mIoU). Crucially, this geometric deprivation causes a sharp decline in downstream spatial intelligence (VSI-Bench drops 4.8%) and VLA performance (CALVIN drops 0.46), validating that explicit 3D priors are prerequisites for Embodied AI. **(iii) vision-language alignment (w/o Captioning)**: While pure vision probing remains stable, omitting the captioning task causes catastrophic failures in VLM integration (VideoMME and VSI-Bench plummet by 9.1% and 12.4%, respectively) and further impacts VLA policy performance. This highlights that early vision-language alignment is critical to bridging the semantic gap.

In conclusion, our unified multitask formulation is not merely a concatenation of independent losses, but a synergistic framework. The semantic (Captioning), dynamic (VideoSSL), and geometric (3D Reconstruction) objectives mutually reinforce the backbone, culminating in a robust representation that excels across both perceptual and embodied tasks.

Model (VLM Backbone)	Carrot	Eggplant	Spoon	Cube	Simpler $\uparrow$
Expert Vision-Language-Action Models					
OpenVLA* (Llama-2) [41]	4.2	0.0	0.0	12.5	4.2
pi0* (Paligemma-1) [14]	62.5	100.0	54.2	25.0	60.4
ThinkAct* (Qwen2.5VL-7B) [35]	37.5	70.8	58.3	8.7	43.8
VLM with VLM4VLA Models (Full Fine-tuning)					
Qwen2.5VL-7B [9]	12.5	100.0	75.0	0.0	46.8
Qwen3VL-8B [8]	58.3	95.8	79.2	0.0	58.3
Paligemma-1-3B [13]	50.0	91.7	75.0	4.2	55.3
Paligemma-2-3B [75]	75.0	75.0	79.2	0.0	57.3
KosMos-2-1.7B [64]	37.5	100.0	75.0	29.2	60.4
VLM with VLM4VLA Models (Frozen Vision)					
Qwen2.5VL-7B	4.2	66.6	4.2	0.0	18.5
LLaVA-Video-7B	0.0	<b>87.5</b>	33.3	0.0	30.2
<b>OmniStream-7B</b>	<b>33.3</b>	83.3	<b>41.7</b>	<b>25.0</b>	<b>45.8</b>

**Table 7 Comparison on SimplerEnv-Bridge.** Entries marked with \* are expert VLAs modified in VLM4VLA settings.

Method	Video Probing		Image Probing			VLM & VLA Probing		
	SSv2 ACC@1 $\uparrow$	DAVIS'17 $\mathcal{J}$ & $\mathcal{F}$ -Mean $\uparrow$	ImageNet ACC@1 $\uparrow$	NYUv2 RMSE $\downarrow$	ADE20k mIoU $\uparrow$	VSIBench Acc $\uparrow$	VideoMME Acc $\uparrow$	CALVIN Seq Len $\uparrow$
Ours	<b>69.3</b>	<b>71.6</b>	<u>85.2</u>	<b>0.379</b>	<b>49.6</b>	<u>57.3</u>	<u>54.1</u>	<b>3.80</b>
w/o. VideoSSL	63.0	67.7	<b>85.4</b>	0.420	<u>47.2</u>	<b>57.9</b>	<b>55.8</b>	<u>3.42</u>
w/o. 3D Geometry	<u>68.4</u>	69.7	85.0	0.471	42.3	52.5	53.8	3.34
w/o. Captioning	67.4	<u>71.0</u>	84.4	<u>0.395</u>	46.9	44.9	45.0	2.38

**Table 8 Ablation study for pre-training tasks.** We investigate the contribution of each objective during pre-training stage: *w/o VideoSSL* removes video data in  $\mathcal{L}_{ssl}$ , *w/o 3D Geometry* omits streaming geometric reconstruction, and *w/o Captioning* disables vision-language alignment.

## 5 Conclusion

In this paper, we introduce OmniStream, a unified vision foundation model that integrates causal spatiotemporal attention and 3D-RoPE into a pre-trained Vision Transformer. Through multi-task training on large-scale datasets from diverse sources, our model achieves competitive performance across a broad spectrum of tasks, including image and video probing, streaming geometric reconstruction, general and spatial video question answering, and robotic manipulation. While OmniStream does not uniformly surpass specialized state-of-the-art methods on every benchmark, its consistent competitiveness across such diverse tasks underscores the viability of training a single, versatile vision backbone that generalizes across semantic, spatial, and temporal reasoning. We believe this versatility represents a more meaningful step toward general-purpose visual understanding than benchmark-specific dominance. As our study focuses on validating this unified paradigm, we leave model scaling as a promising future direction that we expect will further close the remaining gaps with task-specific approaches. We hope this work establishes a solid foundation for streaming visual perception, paving the way for more capable interactive and embodied agents.

# OmniStream: Mastering Perception, Reconstruction and Action in Continuous Streams

## Appendix

### A Details of the SSL Objective

We formally give the definitions of our SSL objective, which is a combination of **DINO loss** [20], **iBOT loss** [118], **KoLeo regularizer** [71], and **Gram anchoring** [74].

- **DINO loss.** To capture the global semantic information of the video clip (or image), we first aggregate the sequence of class tokens  $\{\mathbf{z}_{\text{cls},t}\}_{t=1}^T$  via temporal mean pooling:  $\bar{\mathbf{z}}_{\text{cls}} = \frac{1}{T} \sum_{t=1}^T \mathbf{z}_{\text{cls},t}$ . This aggregated representation is then projected to “prototype scores” by the DINO head of the student and teacher, respectively. After applying softmax to get  $p_s$  and softmax with Sinkhorn-Knopp centering for  $p_t$ , the DINO loss minimizes the cross-entropy between these distributions:

$$\mathcal{L}_{\text{DINO}} = - \sum p_t \log p_s. \quad (11)$$

- **iBOT loss.** We mask both image and video local patches given to the student, where different masking strategies are applied accordingly. For image patches, we follow DINO’s protocol and apply random masks, while the video patches are masked using *multi-block protocol* [10]. We then apply the iBOT head to the student’s masked patches and the teacher’s corresponding to the ones masked in the student. Next, we apply softmax and centering as in the **DINO Loss**, and the iBOT objective is:

$$\mathcal{L}_{\text{iBOT}} = - \sum_i^{N_{\text{mask}}} p_{ti} \log p_{si}, \quad (12)$$

where  $i$  are the indices for masked tokens, and  $N_{\text{mask}}$  is the total number of masks in the sample.

- **KoLeo regularizer.** The KoLeo regularizer encourages a uniform distribution of features within a batch. Given a batch of vectors  $(x_1, \dots, x_n)$ , the KoLeo loss is defined as:

$$\mathcal{L}_{\text{KoLeo}} = -\frac{1}{n} \sum_{i=1}^n \log(\rho_{n,i}), \quad (13)$$

where  $\rho_{n,i} = \min_{j \neq i} \|x_i - x_j\|$  is the minimum distance of  $x_i$  to any other point within the batch.

- **Gram anchoring.** To maintain a consistent patch-level feature during training, we introduce a loss that operates on the gram matrix. The gram matrix is defined as the matrix of all pairwise dot products within the current image. At the beginning of the training, we select the pre-trained DINOv3 as our gram teacher. Given an image sequence of  $hw$  patches,  $\mathbf{X}_s \in \mathbb{R}^{hw \times d}$  denotes the L2-normalized local patch features, and correspondingly for the gram teacher’s local patch features  $\mathbf{X}_g \in \mathbb{R}^{hw \times d}$ . We define the loss as:

$$\mathcal{L}_{\text{gram}} = \|\mathbf{X}_s \cdot \mathbf{X}_s^\top - \mathbf{X}_g \cdot \mathbf{X}_g^\top\|_{\text{F}}^2. \quad (14)$$

Note that we only enable this term for the global crops of the image inputs.

As mentioned in the main text, we optimize the following loss for **static and temporal representation learning**:

$$\mathcal{L}_{\text{ssl}} = \mathcal{L}_{\text{DINO}} + \mathcal{L}_{\text{iBOT}} + 0.1 \times \mathcal{L}_{\text{KoLeo}} + \mathcal{L}_{\text{gram}}, \quad (15)$$

### B Computational Efficiency and Scaling Analysis

To demonstrate the real-world deployment viability and the efficiency of our causal streaming design, we conduct a comprehensive computational analysis comparing OmniStream (utilizing the causal KV-cache)

against a standard bi-directional recomputation baseline. The evaluation is performed on a single NVIDIA H800 GPU with a batch size of 1 and an input resolution of  $224 \times 224$ . Our attention mechanism is implemented using Scaled Dot Product Attention (SDPA) leveraging FlashAttention [24] kernels.

**Temporal Context Expansion and Memory Efficiency.** The ability to process video streams under tight resource constraints is a core strength of OmniStream. We benchmark the per-frame inference latency and peak VRAM consumption for the  $T$ -th frame given a historical context of  $T - 1$  frames (Fig. 3 and Tab. 9).

For the baseline employing full bi-directional recomputation, both latency and memory usage grow prohibitively. Specifically, the recomputation latency reaches nearly 1 second (0.998s) at  $T = 64$ , and the system encounters a catastrophic Out-of-Memory (OOM) error at  $T = 128$  due to the quadratic growth of the attention map.

In contrast, OmniStream utilizes a persistent KV-cache mechanism, resulting in a significantly optimized resource profile. At  $T = 64$ , our model is approximately  $15\times$  faster than the baseline with only 0.067s latency. More importantly, OmniStream maintains a linear and manageable memory growth, effectively preventing OOM even when the context extends to  $T = 512$ . This efficiency ensures that the backbone leaves sufficient VRAM for downstream VLM heads or real-time policy execution on embodied platforms.

Context Length $T$		16	32	64	128	256	512
Full Recompute (Bi-directional)	Latency (s)	0.125	0.329	0.998	N/A	N/A	N/A
	Memory (GB)	3.46	5.95	15.14	OOM	OOM	OOM
<b>OmniStream (KV-cache)</b>	<b>Latency (s)</b>	<b>0.042</b>	<b>0.057</b>	<b>0.067</b>	<b>0.115</b>	<b>0.216</b>	<b>0.414</b>
	<b>Memory (GB)</b>	<b>3.60</b>	<b>4.81</b>	<b>7.26</b>	<b>12.14</b>	<b>21.92</b>	<b>41.46</b>

**Table 9 Inference Efficiency with Varying Context Lengths.** We report the per-frame latency (s) and peak VRAM (GB) for the  $T$ -th frame. Bi-di recomputes the entire sequence, while OmniStream uses a persistent KV-cache.

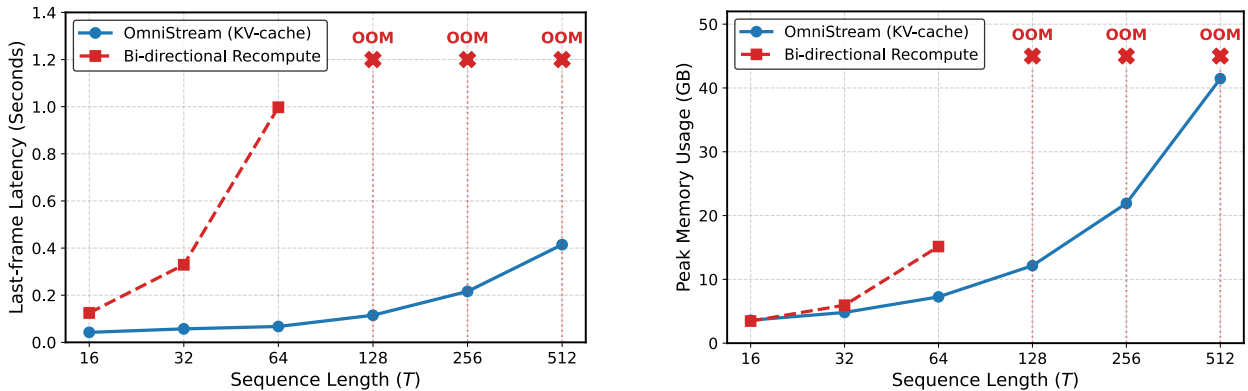


**Figure 3 Qualitative results on Sintel video depth reconstruction.** Our model maintains temporal coherence across long sequences.

## C Details of Downstream Tasks

### C.1 Image Probing Details

To evaluate the static representation quality of our model, we perform linear probing on three standard benchmarks: ImageNet-1K [26] for image classification, NYUv2 [73] for monocular depth estimation, and ADE20K [117] for semantic segmentation. For all tasks, we train a task-specific linear head on top of the strictly frozen visual backbone.

We closely follow the evaluation protocols and configurations of DINOv3 [74]. Detailed hyperparameters are summarized in Tab. 10. Note that for ImageNet classification, we conduct a hyperparameter sweep over 13 learning rate configurations, ranging from  $1 \times 10^{-5}$  to  $1 \times 10^{-1}$ , to report the optimal performance.

Hyperparameters	Dataset Name		
	ImageNet-1K	NYUv2	ADE-20K
Resolution	224 × 224	416 × 544	512 × 512
Learning Rate	$\{1 \times 10^{-5}, \dots, 1 \times 10^{-1}\}$	$1 \times 10^{-3}$	$1 \times 10^{-3}$
Warm-up Steps	0	12,800	1,500
Total Steps	12,500	38,400	40,000

**Table 10** Linear probing detailed configurations.

## C.2 Video Probing Details

To evaluate the dynamic spatiotemporal representation quality of our model, we perform attentive probing on two standard video action recognition benchmarks: Kinetics-400 (K400) [21] and Something-Something V2 (SSv2) [32]. Following V-JEPA 2 [6], we train a lightweight attentive probe—consisting of 4 Transformer blocks with 16 attention heads—on top of the strictly frozen visual backbone.

During training, we sample 16 frames with a frame stride of 4 for both datasets. During inference, we follow the standard multi-view testing protocol, taking multiple temporal segments and spatial crops to obtain the final video-level prediction. Detailed configurations and evaluation protocols are summarized in Tab. 11.

Hyperparameters	Dataset Name	
	Kinetics-400	Something-Something V2
Input Resolution	256 × 256	256 × 256
Frames × Stride	16 × 4	16 × 4
Training Epochs	20	20
Warm-up Epochs	0	0
Learning Rate	$\{1 \times 10^{-4}, 3 \times 10^{-4}\}$	$3 \times 10^{-4}$
Test Segments × Crops	8 × 3	2 × 3

**Table 11** Attentive probing detailed configurations for video action recognition.

Furthermore, we evaluate dense spatiotemporal tracking on the DAVIS’17 [65] Video Object Segmentation (VOS) benchmark, utilizing the standard 480p resolution.

During the dense feature extraction stage, we employ distinct inference strategies tailored to each model’s architectural characteristics: For OmniStream, we fully leverage our causal KV-cache mechanism to encode the entire video sequence in a single continuous stream. This allows the model to maintain long-term temporal coherence effortlessly. In contrast, for the V-JEPA 2 baseline, which relies on a rigid spatiotemporal tubelet size of  $2 \times 16 \times 16$ , we conduct the evaluation using a 16-frame sliding window. To maintain frame-by-frame temporal consistency and accommodate its temporal downsampling mechanism, we explicitly duplicate the input frames. Lastly, for the DINOv3 baseline, we simply adopt a standard per-frame feature extraction.

## C.3 VLM Probing Details

During the VLM training experiments, we adopt the LLaVA-Video [114] pipeline and freeze our vision model throughout all training stages, as given in Tab. 12. We first perform a three-stage fine-tuning following LLaVA-SI [45], which is also the base model for LLaVA-Video. We make sure the same exposure to general video data as LLaVA-Video, where we use a mixture of datasets of LLaVA-Video-178K [114], ActivityNet-QA [108], NExT-QA [96], Perception Test [63], LLaVA-Hound-255K [113], and LLaVA-OV-1.1M [45]. For spatial video QA, we use a combination of VLM-3R-200K [27], VSI-590K [105], and ViCA-322K [28], resulting in a total of 1.1M spatial video QA samples.

We set the base resolution of our visual encoder to 512, which is how our backbone is trained, and adopt the AnyRes-Max strategy [45] for image inputs. For videos, we apply a  $2 \times 2$  average pooling function to each frame and sample at FPS=1 with max frames during training being 32. For VLM training in our ablation

		Stage-1	Stage-1.5	Stage-2	Stage-3
				Single-Image	Video
Vision	Resolution	512	$512 \times \{2 \times 2, 1 \times \{2, 3\}, \{2, 3\} \times 1\}$	$512 \times \{\{1 \times 1\}, \dots, \{6 \times 6\}\}$	$512 \times 32$ ( <i>Frames</i> )
	#Tokens	1024	Max $1024 \times 5$	Max $1024 \times 10$	Max $1024/4 \times 32$
Data	Dataset	LCS	LLaVA-OV-Caption [45]	LLaVA-OV-SI [45]	LLaVA-Video [114] & Spatial QA
	#Samples	558K	4M	3.2M	2.9M + 1.1M
Model	Trainable	Projector	Projector + LLM	Projector + LLM	Projector + LLM
	Qwen2.5-7B	20.0M	7.6B	7.6B	7.6B
Training	Batch Size	512	256	256	128
	LR: $\psi_{\text{vision}}$	N/A	N/A	N/A	N/A
	LR: $\{\theta_{\text{proj}}, \phi_{\text{LLM}}\}$	$1 \times 10^{-3}$	$1 \times 10^{-5}$	$1 \times 10^{-5}$	$1 \times 10^{-5}$
	Epoch	1	1	1	1

**Table 12** Detailed configuration for each training stage of our OmniStream-7B.

study, all stages except stage 1 are sub-sampled at 10% of the total training samples. We run all experiments using  $32 \times$  NVIDIA H200 GPUs.

#### C.4 VLA Probing Details

Hyperparameters	Benchmark	
	CALVIN (ABC-D)	BridgeV2
Input Resolution	$224 \times 224$	$224 \times 224$
Action Space	Continuous (7-DoF)	Continuous (7-DoF)
Optimizer	Adam	Adam
Learning Rate	$2 \times 10^{-5}$	$2 \times 10^{-5}$
Projector Learning Rate	$1 \times 10^{-4}$	$1 \times 10^{-4}$
Gradient Clip Value	1.0	1.0
Batch Size per GPU	8	8
Gradient Accumulation	2	8
Total Epochs	5	5

**Table 13** Detailed VLA fine-tuning configurations for CALVIN and BridgeV2.

To evaluate the capability of our model in embodied control, we adopt the training pipeline introduced by VLM4VLA [112]. Specifically, we evolve our integrated Vision-Language Model (OmniStream-7B, built upon Qwen2.5-7B-Instruct) into a Vision-Language-Action (VLA) model. This is achieved by appending a learnable query token at the end of the input sequence to aggregate action-oriented semantics, followed by a lightweight MLP action head to decode continuous 7-DoF actions.

In our *frozen vision* experiments, we strictly freeze the visual backbone to evaluate the quality of its pre-trained representations. During the VLA fine-tuning phase, we optimize the multimodal projector, the Large Language Model (LLM), the text embeddings, and the newly initialized action head.

We conduct evaluations on two standard robotic manipulation benchmarks: CALVIN (Task ABC-D) and SimplerEnv-BridgeV2. The training is performed using the Adam optimizer with bfloat16 precision and DeepSpeed ZeRO-2 optimization. The detailed hyperparameters for both benchmarks are summarized in Tab. 13. We conduct all VLA experiments using  $8 \times$  NVIDIA H200 GPUs.

## D More Qualitative Results

### D.1 Video Depth Visualizations

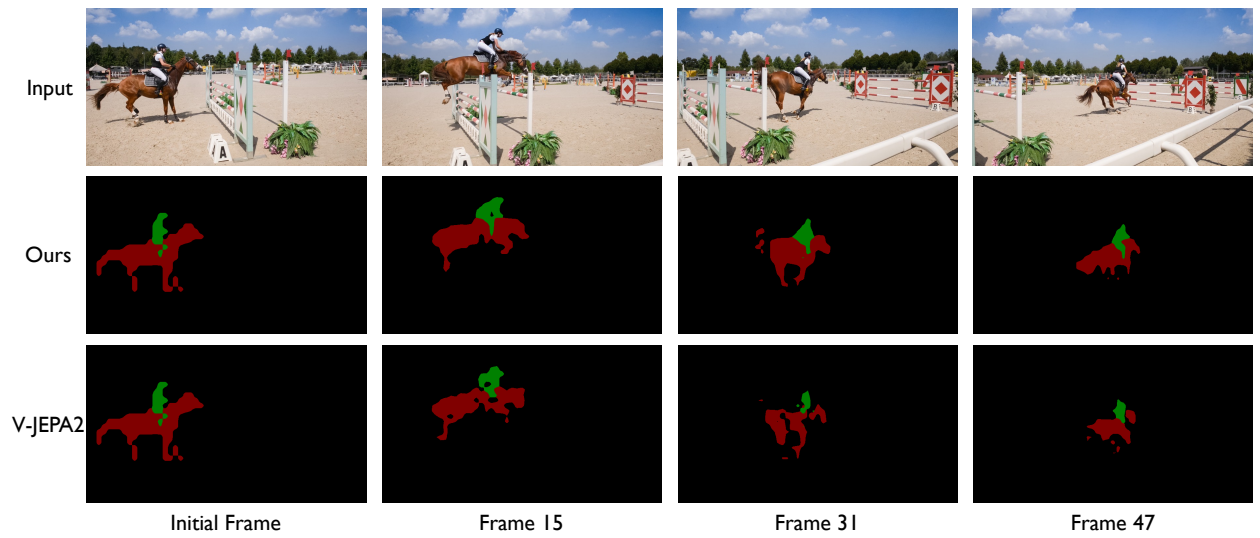
Fig. 4 presents qualitative visualizations of streaming video depth prediction on Sintel[17]. As shown, OmniStream effortlessly maintains high-fidelity spatial details and long-term temporal consistency across highly dynamic scenes.



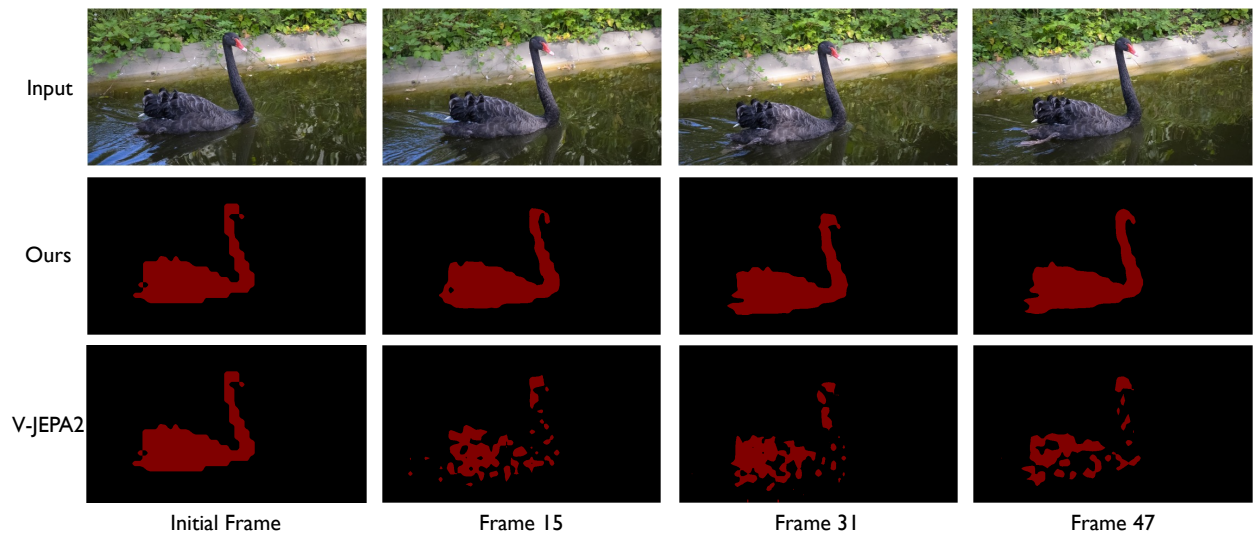
Figure 4 Qualitative results on the Sintel video depth.

### D.2 DAVIS'17 VOS Visualizations

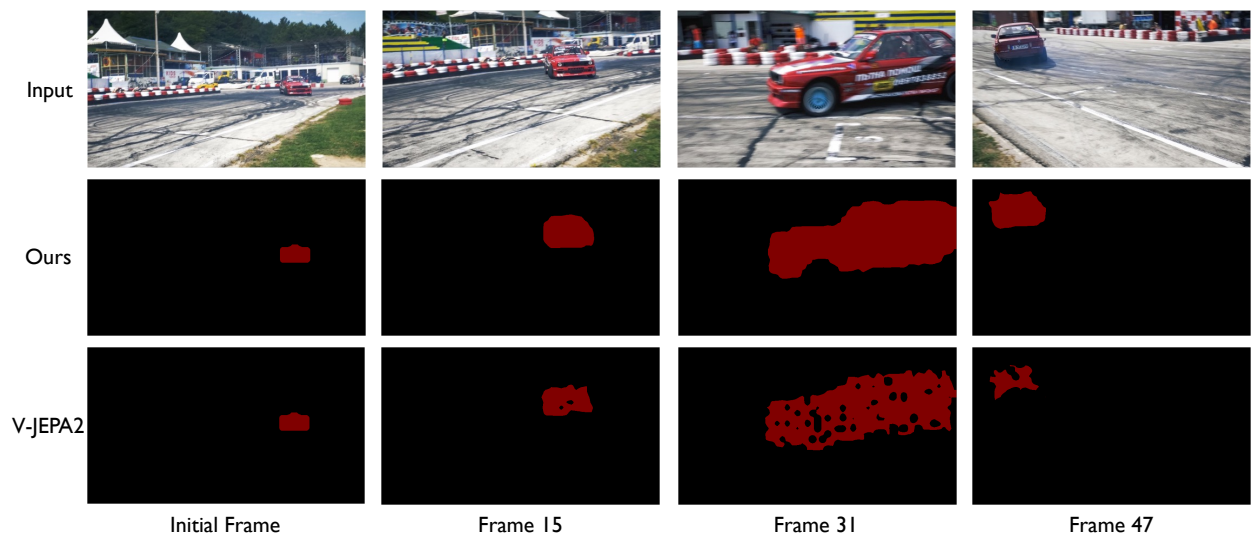
Qualitative results for mask propagation on DAVIS'17 [65] are illustrated in Fig. 5. By leveraging our causal KV-cache for continuous encoding, OmniStream exhibits a pronounced advantage over V-JEPA 2. It successfully tracks intricate object shapes through fast appearance changes, whereas V-JEPA 2 frequently loses dense spatial alignment under sliding-window inference.



(a) horsejump-high sequence.



(b) blackswan sequence.



(c) drift-straight sequence.

Figure 5 Qualitative results on the DAVIS'17 benchmark.

## References

- [1] Josh Achiam, Steven Adler, Sandhini Agarwal, Lama Ahmad, Ilge Akkaya, Florencia Leoni Aleman, Diogo Almeida, Janko Altmerschmidt, Sam Altman, Shyamal Anadkat, et al. Gpt-4 technical report. *arXiv preprint arXiv:2303.08774*, 2023. 1
- [2] Xiang An, Yin Xie, Kaicheng Yang, Wenkang Zhang, Xiuwei Zhao, Zheng Cheng, Yirui Wang, Songcen Xu, Changrui Chen, Didi Zhu, et al. Llava-onevision-1.5: Fully open framework for democratized multimodal training. *arXiv preprint arXiv:2509.23661*, 2025. 3
- [3] Anurag Arnab, Mostafa Dehghani, Georg Heigold, Chen Sun, Mario Lučić, and Cordelia Schmid. Vivit: A video vision transformer. In *ICCV*, 2021. 3
- [4] Eduardo Arnold, Jamie Wynn, Sara Vicente, Guillermo Garcia-Hernando, Áron Monzspart, Victor Adrian Prisacariu, Daniyar Turmukhambetov, and Eric Brachmann. Map-free visual relocalization: Metric pose relative to a single image. In *ECCV*, 2022. 7
- [5] Mahmoud Assran, Quentin Duval, Ishan Misra, Piotr Bojanowski, Pascal Vincent, Michael Rabbat, Yann LeCun, and Nicolas Ballas. Self-supervised learning from images with a joint-embedding predictive architecture. In *ICCV*, 2023. 3
- [6] Mido Assran, Adrien Bardes, David Fan, Quentin Garrido, Russell Howes, Matthew Muckley, Ammar Rizvi, Claire Roberts, Koustuv Sinha, Artem Zhohus, et al. V-jepa 2: Self-supervised video models enable understanding, prediction and planning. *arXiv preprint arXiv:2506.09985*, 2025. 1, 3, 7, 14
- [7] Jinze Bai, Shuai Bai, Yunfei Chu, Zeyu Cui, Kai Dang, Xiaodong Deng, Yang Fan, Wenbin Ge, Yu Han, Fei Huang, et al. Qwen technical report. *arXiv preprint arXiv:2309.16609*, 2023. 3
- [8] Shuai Bai, Yuxuan Cai, Ruizhe Chen, Keqin Chen, Xionghui Chen, Zesen Cheng, Lianghao Deng, Wei Ding, Chang Gao, Chunjiang Ge, et al. Qwen3-vl technical report. *arXiv preprint arXiv:2511.21631*, 2025. 3, 5, 10, 11
- [9] Shuai Bai, Keqin Chen, Xuejing Liu, Jialin Wang, Wenbin Ge, Sibao Song, Kai Dang, Peng Wang, Shijie Wang, Jun Tang, et al. Qwen2. 5-vl technical report. *arXiv preprint arXiv:2502.13923*, 2025. 3, 10, 11
- [10] Adrien Bardes, Quentin Garrido, Jean Ponce, Xinlei Chen, Michael Rabbat, Yann LeCun, Mahmoud Assran, and Nicolas Ballas. Revisiting feature prediction for learning visual representations from video. *arXiv preprint arXiv:2404.08471*, 2024. 1, 3, 12
- [11] Gilad Baruch, Zhuoyuan Chen, Afshin Dehghan, Yuri Feigin, Peter Fu, Thomas Gebauer, Daniel Kurz, Tal Dimry, Brandon Joffe, Arik Schwartz, et al. Arkitscenes: A diverse real-world dataset for 3d indoor scene understanding using mobile rgb-d data. In *NeurIPS*, 2021. 7
- [12] Gedas Bertasius, Heng Wang, and Lorenzo Torresani. Is space-time attention all you need for video understanding? In *ICML*, 2021. 3
- [13] Lucas Beyer, Andreas Steiner, André Susano Pinto, Alexander Kolesnikov, Xiao Wang, Daniel Salz, Maxim Neumann, Ibrahim Alabdulmohsin, Michael Tschannen, Emanuele Bugliarello, et al. Paligemma: A versatile 3b vlm for transfer. *arXiv preprint arXiv:2407.07726*, 2024. 10, 11
- [14] Kevin Black, Noah Brown, Danny Driess, Adnan Esmail, Michael Equi, Chelsea Finn, Niccolò Fusai, Lachy Groom, Karol Hausman, Brian Ichter, et al.  $\pi_0$ : A vision-language-action flow model for general robot control. *arXiv preprint arXiv:2410.24164*, 2024. 3, 10, 11
- [15] Daniel Bolya, Po-Yao Huang, Peize Sun, Jang Hyun Cho, Andrea Madotto, Chen Wei, Tengyu Ma, Jiale Zhi, Jathushan Rajasegaran, Hanoona Rasheed, et al. Perception encoder: The best visual embeddings are not at the output of the network. *arXiv preprint arXiv:2504.13181*, 2025. 7
- [16] Tom Brown, Benjamin Mann, Nick Ryder, Melanie Subbiah, Jared D Kaplan, Prafulla Dhariwal, Arvind Neelakantan, Pranav Shyam, Girish Sastry, Amanda Askell, et al. Language models are few-shot learners. *NeurIPS*, 2020. 1
- [17] Daniel J Butler, Jonas Wulff, Garrett B Stanley, and Michael J Black. A naturalistic open source movie for optical flow evaluation. In *ECCV*, 2012. 8, 16
- [18] Minwoo Byeon, Beomhee Park, Haecheon Kim, Sungjun Lee, Woonhyuk Baek, and Saehoon Kim. Coyo-700m: Image-text pair dataset. <https://github.com/kakaobrain/coyo-dataset>, 2022. 7

- [19] Yohann Cabon, Naila Murray, and Martin Humenberger. Virtual kitti 2. *arXiv preprint arXiv:2001.10773*, 2020. [7](#)
- [20] Mathilde Caron, Hugo Touvron, Ishan Misra, Hervé Jégou, Julien Mairal, Piotr Bojanowski, and Armand Joulin. Emerging properties in self-supervised vision transformers. In *ICCV*, 2021. [3](#), [5](#), [12](#)
- [21] Joao Carreira and Andrew Zisserman. Quo vadis, action recognition? a new model and the kinetics dataset. In *CVPR*, 2017. [7](#), [14](#)
- [22] Zhe Chen, Weiyun Wang, Hao Tian, Shenglong Ye, Zhangwei Gao, Erfei Cui, Wenwen Tong, Kongzhi Hu, Jiapeng Luo, Zheng Ma, et al. How far are we to gpt-4v? closing the gap to commercial multimodal models with open-source suites. *arXiv preprint arXiv:2404.16821*, 2024. [7](#)
- [23] Angela Dai, Angel X. Chang, Manolis Savva, Maciej Halber, Thomas Funkhouser, and Matthias Nießner. Scannet: Richly-annotated 3d reconstructions of indoor scenes. In *CVPR*, 2017. [7](#), [8](#)
- [24] Tri Dao, Dan Fu, Stefano Ermon, Atri Rudra, and Christopher Ré. Flashattention: Fast and memory-efficient exact attention with io-awareness. *NeurIPS*, 2022. [13](#)
- [25] Timothée Darcet, Maxime Oquab, Julien Mairal, and Piotr Bojanowski. Vision transformers need registers. In *ICLR*, 2024. [4](#)
- [26] Jia Deng, Wei Dong, Richard Socher, Li-Jia Li, Kai Li, and Li Fei-Fei. Imagenet: A large-scale hierarchical image database. In *CVPR*, 2009. [1](#), [7](#), [13](#)
- [27] Zhiwen Fan, Jian Zhang, Renjie Li, Junge Zhang, Runjin Chen, Hezhen Hu, Kevin Wang, Huaizhi Qu, Dilin Wang, Zhicheng Yan, et al. Vlm-3r: Vision-language models augmented with instruction-aligned 3d reconstruction. *arXiv preprint arXiv:2505.20279*, 2025. [3](#), [9](#), [10](#), [14](#)
- [28] Qi Feng. Towards visuospatial cognition via hierarchical fusion of visual experts. *arXiv preprint arXiv:2505.12363*, 2025. [14](#)
- [29] Chaoyou Fu, Yuhan Dai, Yongdong Luo, Lei Li, Shuhuai Ren, Renrui Zhang, Zihan Wang, Chenyu Zhou, Yunhang Shen, Mengdan Zhang, et al. Video-mme: The first-ever comprehensive evaluation benchmark of multi-modal llms in video analysis. In *CVPR*, 2025. [9](#)
- [30] Samir Yitzhak Gadre, Gabriel Ilharco, Alex Fang, Jonathan Hayase, Georgios Smyrnis, Thao Nguyen, Ryan Marten, Mitchell Wortsman, Dhruva Ghosh, Jieyu Zhang, et al. Datacomp: In search of the next generation of multimodal datasets. *NeurIPS*, 2023. [7](#)
- [31] Andreas Geiger, Philip Lenz, Christoph Stiller, and Raquel Urtasun. Vision meets robotics: The kitti dataset. *International Journal of Robotics Research*, 2013. [8](#)
- [32] Raghav Goyal, Samira Ebrahimi Kahou, Vincent Michalski, Joanna Materzynska, Susanne Westphal, Heuna Kim, Valentin Haenel, Ingo Fruend, Peter Yianilos, Moritz Mueller-Freitag, et al. The "something something" video database for learning and evaluating visual common sense. In *ICCV*, 2017. [7](#), [14](#)
- [33] Kaiming He, Xinlei Chen, Saining Xie, Yanghao Li, Piotr Dollár, and Ross Girshick. Masked autoencoders are scalable vision learners. In *ICCV*, 2022. [3](#)
- [34] Kairui Hu, Penghao Wu, Fanyi Pu, Wang Xiao, Yuanhan Zhang, Xiang Yue, Bo Li, and Ziwei Liu. Video-mmmu: Evaluating knowledge acquisition from multi-discipline professional videos. *arXiv preprint arXiv:2501.13826*, 2025. [9](#)
- [35] Chi-Pin Huang, Yueh-Hua Wu, Min-Hung Chen, Yu-Chiang Frank Wang, and Fu-En Yang. Thinkact: Vision-language-action reasoning via reinforced visual latent planning. *arXiv preprint arXiv:2507.16815*, 2025. [11](#)
- [36] Po-Han Huang, Kevin Matzen, Johannes Kopf, Narendra Ahuja, and Jia-Bin Huang. Deepmvs: Learning multi-view stereopsis. In *CVPR*, 2018. [7](#)
- [37] Aaron Hurst, Adam Lerer, Adam P Goucher, Adam Perelman, Aditya Ramesh, Aidan Clark, AJ Ostrow, Akila Welihinda, Alan Hayes, Alec Radford, et al. Gpt-4o system card. *arXiv preprint arXiv:2410.21276*, 2024. [10](#)
- [38] Oğuzhan Fatih Kar, Alessio Tonioni, Petra Poklukar, Achin Kulshrestha, Amir Zamir, and Federico Tombari. Brave: Broadening the visual encoding of vision-language models. In *ECCV*, 2024. [3](#)
- [39] Nikita Karaev, Ignacio Rocco, Benjamin Graham, Natalia Neverova, Andrea Vedaldi, and Christian Rupprecht. Dynamicstereo: Consistent dynamic depth from stereo videos. *CVPR*, 2023. [7](#)

- [40] Sahar Kazemzadeh, Vicente Ordonez, Mark Matten, and Tamara Berg. Referitgame: Referring to objects in photographs of natural scenes. In *EMNLP*, 2014. 7
- [41] Moo Jin Kim, Karl Pertsch, Siddharth Karamcheti, Ted Xiao, Ashwin Balakrishna, Suraj Nair, Rafael Rafailov, Ethan Foster, Grace Lam, Pannag Sanketi, Quan Vuong, Thomas Kollar, Benjamin Burchfiel, Russ Tedrake, Dorsa Sadigh, Sergey Levine, Percy Liang, and Chelsea Finn. Openvla: An open-source vision-language-action model. *arXiv preprint arXiv:2406.09246*, 2024. 3, 10, 11
- [42] Diederik P. Kingma and Jimmy Ba. Adam: A method for stochastic optimization. In *ICLR*, 2015. 7
- [43] Alexander Kirillov, Eric Mintun, Nikhila Ravi, Hanzi Mao, Chloe Rolland, Laura Gustafson, Tete Xiao, Spencer Whitehead, Alexander C Berg, Wan-Yen Lo, et al. Segment anything. In *ICCV*, 2023. 1
- [44] Yushi Lan, Yihang Luo, Fangzhou Hong, Shangchen Zhou, Honghua Chen, Zhaoyang Lyu, Shuai Yang, Bo Dai, Chen Change Loy, and Xingang Pan. Stream3r: Scalable sequential 3d reconstruction with causal transformer. *arXiv preprint arXiv:2508.10893*, 2025. 3
- [45] Bo Li, Yuanhan Zhang, Dong Guo, Renrui Zhang, Feng Li, Hao Zhang, Kaichen Zhang, Peiyuan Zhang, Yanwei Li, Ziwei Liu, et al. Llava-onevision: Easy visual task transfer. *arXiv preprint arXiv:2408.03326*, 2024. 3, 10, 14, 15
- [46] Xuanlin Li, Kyle Hsu, Jiayuan Gu, Oier Mees, Karl Pertsch, Homer Rich Walke, Chuyuan Fu, Ishikaa Lunawat, Isabel Sieh, Sean Kirmani, et al. Evaluating real-world robot manipulation policies in simulation. In *CoRL*, 2024. 9
- [47] Xinghang Li, Peiyan Li, Minghuan Liu, Dong Wang, Jirong Liu, Bingyi Kang, Xiao Ma, Tao Kong, Hanbo Zhang, and Huaping Liu. Towards generalist robot policies: What matters in building vision-language-action models. *arXiv preprint arXiv:2412.14058*, 2024. 3
- [48] Zhengqi Li and Noah Snavely. Megadepth: Learning single-view depth prediction from internet photos. In *CVPR*, 2018. 7
- [49] Haotong Lin, Sili Chen, Junhao Liew, Donny Y Chen, Zhenyu Li, Guang Shi, Jiashi Feng, and Bingyi Kang. Depth anything 3: Recovering the visual space from any views. *arXiv preprint arXiv:2511.10647*, 2025. 1, 3, 5
- [50] Lu Ling, Yichen Sheng, Zhi Tu, Wentian Zhao, Cheng Xin, Kun Wan, Lantao Yu, Qianyu Guo, Zixun Yu, Yawen Lu, et al. D13dv-10k: A large-scale scene dataset for deep learning-based 3d vision. In *CVPR*, 2024. 7
- [51] Haotian Liu, Chunyuan Li, Qingyang Wu, and Yong Jae Lee. Visual instruction tuning. *NeurIPS*, 2023. 3
- [52] Haotian Liu, Chunyuan Li, Yuheng Li, Bo Li, Yuanhan Zhang, Sheng Shen, and Yong Jae Lee. Llava-next: Improved reasoning, ocr, and world knowledge, 2024. 3
- [53] Haoyu Lu, Wen Liu, Bo Zhang, Bingxuan Wang, Kai Dong, Bo Liu, Jingxiang Sun, Tongzheng Ren, Zhuoshu Li, Hao Yang, et al. Deepseek-vl: towards real-world vision-language understanding. *arXiv preprint arXiv:2403.05525*, 2024. 3
- [54] Jiasen Lu, Christopher Clark, Rowan Zellers, Roozbeh Mottaghi, and Aniruddha Kembhavi. Unified-io: A unified model for vision, language, and multi-modal tasks. *arXiv preprint arXiv:2206.08916*, 2022. 1
- [55] Jiasen Lu, Christopher Clark, Sangho Lee, Zichen Zhang, Savya Khosla, Ryan Marten, Derek Hoiem, and Aniruddha Kembhavi. Unified-io 2: Scaling autoregressive multimodal models with vision language audio and action. In *CVPR*, 2024. 1
- [56] Karttikeya Mangalam, Raiymbek Akshulakov, and Jitendra Malik. Egoschema: A diagnostic benchmark for very long-form video language understanding. *NeurIPS*, 2023. 9
- [57] Oier Mees, Lukas Hermann, Erick Rosete-Beas, and Wolfram Burgard. Calvin: A benchmark for language-conditioned policy learning for long-horizon robot manipulation tasks. *IEEE-RAL*, 2022. 9
- [58] Lukas Mehl, Jenny Schmalfluss, Azin Jahedi, Yaroslava Nalivayko, and Andrés Bruhn. Spring: A high-resolution high-detail dataset and benchmark for scene flow, optical flow and stereo. In *CVPR*, 2023. 7
- [59] Maxime Oquab, Timothée Darcet, Théo Moutakanni, Huy Vo, Marc Szafraniec, Vasil Khalidov, Pierre Fernandez, Daniel Haziza, Francisco Massa, Alaaeldin El-Nouby, et al. Dinov2: Learning robust visual features without supervision. *arXiv preprint arXiv:2304.07193*, 2023. 1, 3
- [60] Kun Ouyang, Yuanxin Liu, Haoning Wu, Yi Liu, Hao Zhou, Jie Zhou, Fandong Meng, and Xu Sun. Spacer: Reinforcing mllms in video spatial reasoning. *arXiv preprint arXiv:2504.01805*, 2025. 10

- [61] Emanuele Palazzolo, Jens Behley, Philipp Lottes, Philippe Giguere, and Cyrill Stachniss. Refusion: 3d reconstruction in dynamic environments for rgb-d cameras exploiting residuals. In *IROS*, 2019. 8
- [62] Xiaqing Pan, Nicholas Charron, Yongqian Yang, Scott Peters, Thomas Whelan, Chen Kong, Omkar Parkhi, Richard Newcombe, and Yuheng Carl Ren. Aria digital twin: A new benchmark dataset for egocentric 3d machine perception. In *ICCV*, 2023. 7
- [63] Viorica Patraucean, Lucas Smaira, Ankush Gupta, Adria Recasens, Larisa Markeeva, Dylan Banarse, Skanda Koppula, Mateusz Malinowski, Yi Yang, Carl Doersch, et al. Perception test: A diagnostic benchmark for multimodal video models. *NeurIPS*, 2023. 9, 14
- [64] Zhiliang Peng, Wenhui Wang, Li Dong, Yaru Hao, Shaohan Huang, Shuming Ma, and Furu Wei. Kosmos-2: Grounding multimodal large language models to the world. *ArXiv*, 2023. 7, 10, 11
- [65] Jordi Pont-Tuset, Federico Perazzi, Sergi Caelles, Pablo Arbeláez, Alex Sorkine-Hornung, and Luc Van Gool. The 2017 davis challenge on video object segmentation. *arXiv preprint arXiv:1704.00675*, 2017. 7, 14, 16
- [66] Qwen, :, An Yang, Baosong Yang, Beichen Zhang, Binyuan Hui, Bo Zheng, Bowen Yu, Chengyuan Li, Dayiheng Liu, Fei Huang, Haoran Wei, Huan Lin, Jian Yang, Jianhong Tu, Jianwei Zhang, Jianxin Yang, Jiayi Yang, Jingren Zhou, Junyang Lin, Kai Dang, Keming Lu, Keqin Bao, Kexin Yang, Le Yu, Mei Li, Mingfeng Xue, Pei Zhang, Qin Zhu, Rui Men, Runji Lin, Tianhao Li, Tianyi Tang, Tingyu Xia, Xingzhang Ren, Xuancheng Ren, Yang Fan, Yang Su, Yichang Zhang, Yu Wan, Yuqiong Liu, Zeyu Cui, Zhenru Zhang, and Zihan Qiu. Qwen2.5 technical report, 2025. 9
- [67] Alec Radford, Jong Wook Kim, Chris Hallacy, Aditya Ramesh, Gabriel Goh, Sandhini Agarwal, Girish Sastry, Amanda Askell, Pamela Mishkin, Jack Clark, et al. Learning transferable visual models from natural language supervision. In *ICML*, 2021. 3
- [68] Jeremy Reizenstein, Roman Shapovalov, Philipp Henzler, Luca Sbordone, Patrick Labatut, and David Novotny. Common objects in 3d: Large-scale learning and evaluation of real-life 3d category reconstruction. In *ICCV*, 2021. 7
- [69] Tal Ridnik, Emanuel Ben-Baruch, Asaf Noy, and Lih Zelnik-Manor. Imagenet-21k pretraining for the masses. *arXiv preprint arXiv:2104.10972*, 2021. 7
- [70] Mike Roberts, Jason Ramapuram, Anurag Ranjan, Atulit Kumar, Miguel Angel Bautista, Nathan Paczan, Russ Webb, and Joshua M Susskind. Hypersim: A photorealistic synthetic dataset for holistic indoor scene understanding. In *ICCV*, 2021. 7
- [71] Alexandre Sablayrolles, Matthijs Douze, Cordelia Schmid, and Hervé Jégou. Spreading vectors for similarity search. *arXiv preprint arXiv:1806.03198*, 2018. 5, 12
- [72] Min Shi, Fuxiao Liu, Shihao Wang, Shijia Liao, Subhashree Radhakrishnan, Yilin Zhao, De-An Huang, Hongxu Yin, Karan Sapra, Yaser Yacoob, et al. Eagle: Exploring the design space for multimodal llms with mixture of encoders. *arXiv preprint arXiv:2408.15998*, 2024. 3
- [73] Nathan Silberman, Derek Hoiem, Pushmeet Kohli, and Rob Fergus. Indoor segmentation and support inference from rgb-d images. In *ECCV*, 2012. 7, 13
- [74] Oriane Siméoni, Huy V Vo, Maximilian Seitzer, Federico Baldassarre, Maxime Oquab, Cijo Jose, Vasil Khalidov, Marc Szafraniec, Seungeun Yi, Michaël Ramamonjisoa, et al. Dinov3. *arXiv preprint arXiv:2508.10104*, 2025. 1, 3, 4, 5, 7, 12, 13
- [75] Andreas Steiner, André Susano Pinto, Michael Tschannen, Daniel Keysers, Xiao Wang, Yonatan Bitton, Alexey Gritsenko, Matthias Minderer, Anthony Sherbondy, Shangbang Long, et al. Paligemma 2: A family of versatile vlms for transfer. *arXiv preprint arXiv:2412.03555*, 2024. 10, 11
- [76] Jürgen Sturm, Nikolas Engelhard, Felix Endres, Wolfram Burgard, and Daniel Cremers. A benchmark for the evaluation of rgb-d slam systems. In *IROS*, 2012. 8
- [77] Pei Sun, Henrik Kretzschmar, Xerxes Dotiwalla, Aurelien Chouard, Vijaysai Patnaik, Paul Tsui, James Guo, Yin Zhou, Yuning Chai, Benjamin Caine, Vijay Vasudevan, Wei Han, Jiquan Ngiam, Hang Zhao, Aleksei Timofeev, Scott Ettinger, Maxim Krivokon, Amy Gao, Aditya Joshi, Yu Zhang, Jonathon Shlens, Zhifeng Chen, and Dragomir Anguelov. Scalability in perception for autonomous driving: Waymo open dataset. In *CVPR*, 2020. 7

- [78] Gemini Team, Petko Georgiev, Ving Ian Lei, Ryan Burnell, Libin Bai, Anmol Gulati, Garrett Tanzer, Damien Vincent, Zhufeng Pan, Shibo Wang, et al. Gemini 1.5: Unlocking multimodal understanding across millions of tokens of context. *arXiv preprint arXiv:2403.05530*, 2024. 10
- [79] Peter Tong, Ellis Brown, Penghao Wu, Sanghyun Woo, Adithya Jairam Vedagiri IYER, Sai Charitha Akula, Shusheng Yang, Jihan Yang, Manoj Middepogu, Ziteng Wang, et al. Cambrian-1: A fully open, vision-centric exploration of multimodal llms. In *NeurIPS*, 2024. 3
- [80] Shengbang Tong, Zhuang Liu, Yuexiang Zhai, Yi Ma, Yann LeCun, and Saining Xie. Eyes wide shut? exploring the visual shortcomings of multimodal llms. In *CVPR*, 2024. 3
- [81] Zhan Tong, Yibing Song, Jue Wang, and Limin Wang. Videomae: Masked autoencoders are data-efficient learners for self-supervised video pre-training. *NeurIPS*, 2022. 1, 3
- [82] Michael Tschanen, Alexey Gritsenko, Xiao Wang, Muhammad Ferjad Naeem, Ibrahim Alabdulmohsin, Nikhil Parthasarathy, Talfan Evans, Lucas Beyer, Ye Xia, Basil Mustafa, et al. Siglip 2: Multilingual vision-language encoders with improved semantic understanding, localization, and dense features. *arXiv preprint arXiv:2502.14786*, 2025. 1, 3
- [83] Hengyi Wang and Lourdes Agapito. 3d reconstruction with spatial memory. In *3DV*, 2025. 3, 9
- [84] Jianyuan Wang, Minghao Chen, Nikita Karaev, Andrea Vedaldi, Christian Rupprecht, and David Novotny. Vggt: Visual geometry grounded transformer. In *CVPR*, 2025. 1, 3, 5
- [85] Limin Wang, Bingkun Huang, Zhiyu Zhao, Zhan Tong, Yanan He, Yi Wang, Yali Wang, and Yu Qiao. Videomae v2: Scaling video masked autoencoders with dual masking. In *CVPR*, 2023. 1, 3
- [86] Peng Wang, An Yang, Rui Men, Junyang Lin, Shuai Bai, Zhikang Li, Jianxin Ma, Chang Zhou, Jingren Zhou, and Hongxia Yang. Ofa: Unifying architectures, tasks, and modalities through a simple sequence-to-sequence learning framework. In *ICML*, 2022. 1
- [87] Qianqian Wang\*, Yifei Zhang\*, Aleksander Holynski, Alexei A. Efros, and Angjoo Kanazawa. Continuous 3d perception model with persistent state. In *CVPR*, 2025. 3, 8, 9
- [88] Shuzhe Wang, Vincent Leroy, Yohann Cabon, Boris Chidlovskii, and Jerome Revaud. Dust3r: Geometric 3d vision made easy. In *CVPR*, 2024. 3
- [89] Wenshan Wang, DeLong Zhu, Xiangwei Wang, Yaoyu Hu, Yuheng Qiu, Chen Wang, Yafei Hu, Ashish Kapoor, and Sebastian Scherer. Tartanair: A dataset to push the limits of visual slam. In *IROS*, 2020. 7
- [90] Yizhong Wang, Swaroop Mishra, Pegah Alipoormolabashi, Yeganeh Kordi, Amirreza Mirzaei, Atharva Naik, Arjun Ashok, Arut Selvan Dhanasekaran, Anjana Arunkumar, David Stap, et al. Super-naturalinstructions: Generalization via declarative instructions on 1600+ nlp tasks. In *EMNLP*, 2022. 1
- [91] Yifan Wang, Jianjun Zhou, Haoyi Zhu, Wenzheng Chang, Yang Zhou, Zizun Li, Junyi Chen, Jiangmiao Pang, Chunhua Shen, and Tong He.  $\pi^3$ : Permutation-equivariant visual geometry learning. *arXiv preprint arXiv:2507.13347*, 2025. 3
- [92] Junfei Wu, Jian Guan, Kaituo Feng, Qiang Liu, Shu Wu, Liang Wang, Wei Wu, and Tieniu Tan. Reinforcing spatial reasoning in vision-language models with interwoven thinking and visual drawing. *arXiv preprint arXiv:2506.09965*, 2025. 10
- [93] Yuqi Wu, Wenzhao Zheng, Jie Zhou, and Jiwen Lu. Point3r: Streaming 3d reconstruction with explicit spatial pointer memory. *arXiv preprint arXiv:2507.02863*, 2025. 3, 9
- [94] Hongchi Xia, Yang Fu, Sifei Liu, and Xiaolong Wang. Rgb-d objects in the wild: Scaling real-world 3d object learning from rgb-d videos. In *CVPR*, 2024. 7
- [95] Bin Xiao, Haiping Wu, Weijian Xu, Xiyang Dai, Houdong Hu, Yumao Lu, Michael Zeng, Ce Liu, and Lu Yuan. Florence-2: Advancing a unified representation for a variety of vision tasks. In *CVPR*, 2024. 1
- [96] Junbin Xiao, Xindi Shang, Angela Yao, and Tat-Seng Chua. Next-qa: Next phase of question-answering to explaining temporal actions. In *CVPR*, 2021. 14
- [97] Le Xue, Manli Shu, Anas Awadalla, Jun Wang, An Yan, Senthil Purushwalkam, Honglu Zhou, Viraj Prabhu, Yutong Dai, Michael S Ryoo, et al. xgen-mm (blip-3): A family of open large multimodal models. *arXiv preprint arXiv:2408.08872*, 2024. 7

- [98] Yibin Yan, Jilan Xu, Shangzhe Di, Yikun Liu, Yudi Shi, Qirui Chen, Zeqian Li, Yifei Huang, and Weidi Xie. Learning streaming video representation via multitask training. In *ICCV*, 2025. 3
- [99] An Yang, Anfeng Li, Baosong Yang, Beichen Zhang, Binyuan Hui, Bo Zheng, Bowen Yu, Chang Gao, Chengen Huang, Chenxu Lv, et al. Qwen3 technical report. *arXiv preprint arXiv:2505.09388*, 2025. 6
- [100] Jianing Yang, Alexander Sax, Kevin J Liang, Mikael Henaff, Hao Tang, Ang Cao, Joyce Chai, Franziska Meier, and Matt Feiszli. Fast3r: Towards 3d reconstruction of 1000+ images in one forward pass. In *CVPR*, 2025. 3
- [101] Jihan Yang, Shusheng Yang, Anjali W Gupta, Rilyn Han, Li Fei-Fei, and Saining Xie. Thinking in space: How multimodal large language models see, remember, and recall spaces. In *CVPR*, 2025. 9
- [102] Lihe Yang, Bingyi Kang, Zilong Huang, Xiaogang Xu, Jiashi Feng, and Hengshuang Zhao. Depth anything: Unleashing the power of large-scale unlabeled data. In *CVPR*, 2024. 1
- [103] Lihe Yang, Bingyi Kang, Zilong Huang, Zhen Zhao, Xiaogang Xu, Jiashi Feng, and Hengshuang Zhao. Depth anything v2. *NeurIPS*, 2024. 1
- [104] Rui Yang, Ziyu Zhu, Yanwei Li, Jingjia Huang, Shen Yan, Siyuan Zhou, Zhe Liu, Xiangtai Li, Shuangye Li, Wenqian Wang, et al. Visual spatial tuning. *arXiv preprint arXiv:2511.05491*, 2025. 10
- [105] Shusheng Yang, Jihan Yang, Pinzhi Huang, Ellis Brown, Zihao Yang, Yue Yu, Shengbang Tong, Zihan Zheng, Yifan Xu, Muhan Wang, et al. Cambrian-s: Towards spatial supersensing in video. *arXiv preprint arXiv:2511.04670*, 2025. 14
- [106] Yao Yao, Zixin Luo, Shiwei Li, Jingyang Zhang, Yufan Ren, Lei Zhou, Tian Fang, and Long Quan. Blendedmvs: A large-scale dataset for generalized multi-view stereo networks. *CVPR*, 2020. 7
- [107] Chandan Yeshwanth, Yueh-Cheng Liu, Matthias Nießner, and Angela Dai. Scannet++: A high-fidelity dataset of 3d indoor scenes. In *ICCV*, 2023. 7
- [108] Zhou Yu, Dejing Xu, Jun Yu, Ting Yu, Zhou Zhao, Yueting Zhuang, and Dacheng Tao. Activitynet-qa: A dataset for understanding complex web videos via question answering. In *AAAI*, 2019. 14
- [109] Lu Yuan, Dongdong Chen, Yi-Ling Chen, Noel Codella, Xiyang Dai, Jianfeng Gao, Houdong Hu, Xuedong Huang, Boxin Li, Chunyuan Li, et al. Florence: A new foundation model for computer vision. *arXiv preprint arXiv:2111.11432*, 2021. 1
- [110] Xiaohua Zhai, Basil Mustafa, Alexander Kolesnikov, and Lucas Beyer. Sigmoid loss for language image pre-training. In *ICCV*, 2023. 1, 3
- [111] Chuhan Zhang, Guillaume Le Moing, Skanda Koppula, Ignacio Rocco, Liliane Momeni, Junyu Xie, Shuyang Sun, Rahul Sukthankar, Joëlle K. Barral, Raia Hadsell, Zoubin Ghahramani, Andrew Zisserman, Junlin Zhang, and Mehdi S. M. Sajjadi. Efficiently reconstructing dynamic scenes one d4rt at a time. *arXiv preprint*, 2025. 3
- [112] Jianke Zhang, Xiaoyu Chen, Qiuyue Wang, Mingsheng Li, Yanjiang Guo, Yucheng Hu, Jiajun Zhang, Shuai Bai, Junyang Lin, and Jianyu Chen. Vlm4vla: Revisiting vision-language-models in vision-language-action models. *arXiv preprint arXiv:2601.03309*, 2026. 3, 9, 15
- [113] Ruohong Zhang, Liangke Gui, Zhiqing Sun, Yihao Feng, Keyang Xu, Yuanhan Zhang, Di Fu, Chunyuan Li, Alexander Hauptmann, Yonatan Bisk, et al. Direct preference optimization of video large multimodal models from language model reward. *arXiv preprint arXiv:2404.01258*, 2024. 14
- [114] Yuanhan Zhang, Jinming Wu, Wei Li, Bo Li, Zejun Ma, Ziwei Liu, and Chunyuan Li. Llava-video: Video instruction tuning with synthetic data. *arXiv preprint arXiv:2410.02713*, 2024. 3, 9, 10, 14, 15
- [115] Ruosen Zhao, Zhikang Zhang, Jialei Xu, Jiahao Chang, Dong Chen, Lingyun Li, Weijian Sun, and Zizhuang Wei. Spacemind: Camera-guided modality fusion for spatial reasoning in vision-language models. *arXiv preprint arXiv:2511.23075*, 2025. 3, 9, 10
- [116] Yang Zheng, Adam W. Harley, Bokui Shen, Gordon Wetzstein, and Leonidas J. Guibas. Pointodyssey: A large-scale synthetic dataset for long-term point tracking. In *ICCV*, 2023. 7
- [117] Bolei Zhou, Hang Zhao, Xavier Puig, Sanja Fidler, Adela Barriuso, and Antonio Torralba. Scene parsing through ade20k dataset. In *CVPR*, 2017. 7, 13
- [118] Jinghao Zhou, Chen Wei, Huiyu Wang, Wei Shen, Cihang Xie, Alan Yuille, and Tao Kong. Image bert pre-training with online tokenizer. In *ICLR*, 2022. 5, 12

- [119] Yang Zhou, Yifan Wang, Jianjun Zhou, Wenzheng Chang, Haoyu Guo, Zizun Li, Kaijing Ma, Xinyue Li, Yating Wang, Haoyi Zhu, Mingyu Liu, Dingning Liu, Jiange Yang, Zhoujie Fu, Junyi Chen, Chunhua Shen, Jiangmiao Pang, Kaipeng Zhang, and Tong He. Omniworld: A multi-domain and multi-modal dataset for 4d world modeling. *arXiv preprint arXiv:2509.12201*, 2025. 7
- [120] Dong Zhuo, Wenzhao Zheng, Jiahe Guo, Yuqi Wu, Jie Zhou, and Jiwen Lu. Streaming 4d visual geometry transformer. *arXiv preprint arXiv:2507.11539*, 2025. 3
- [121] Brianna Zitkovich, Tianhe Yu, Sichun Xu, Peng Xu, Ted Xiao, Fei Xia, Jialin Wu, Paul Wohlhart, Stefan Welker, Ayzan Wahid, et al. Rt-2: Vision-language-action models transfer web knowledge to robotic control. In *CoRL*, 2023. 3